Figure 3. MG132 and 17-AAG inhibition of HCV RNA replication in HCV replicon cells

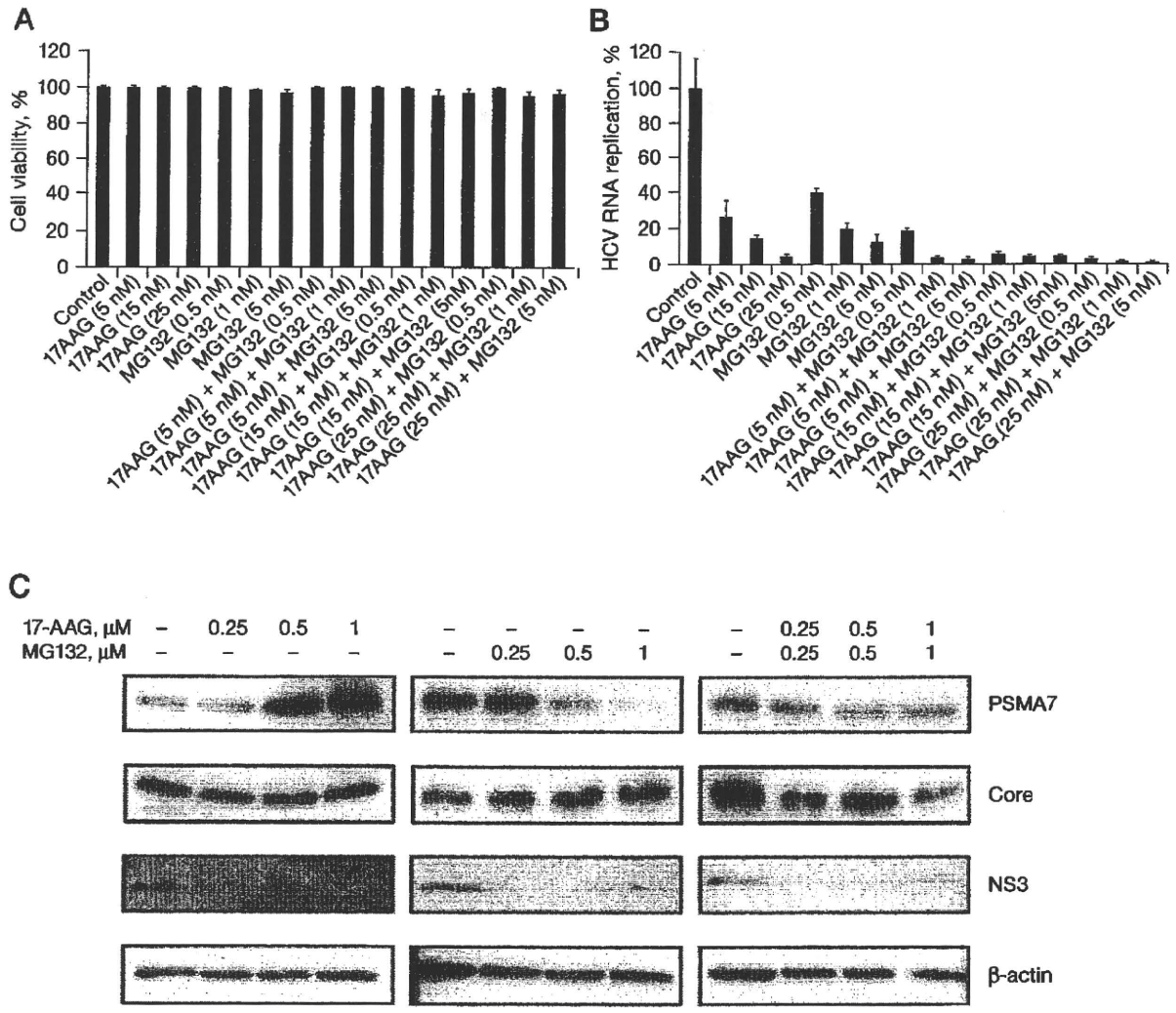

(A) Cytotoxic effects of 17-AAG and MG132, singly or in combination, on NNC#2 cells, shown as the percentage reduction of the number of viable cells assessed by MTS assay. Data are means ±SD of triplicate experiments. (B) Inhibition of hepatitis C virus (HCV) replication by 17-AAG and MG132, singly or in combination, in NNC#2 cells. Measurement of HCV replication by real-time reverse transcriptase PCR. Data are means ±SD of triplicate experiments. (C) Effect of 17-AAG and MG132 on the expression of core, non-structural protein 3 (NS3) and the proteasome α-subunit 7 (PSMA7) protein. The core, NS3 and PSMA7 protein were analysed by western blotting after treatment of NNC#2 cells with various concentrations of 17-AAG or MG132, alone or in combination. β-Actin was used as a lysate control.

with various concentrations of 17-AAG or MG132 alone, and 17-AAG plus MG132 at day 2. Treatment with 17-AAG alone increased the expression of PSMA7, but did not reduce core protein expression. By contrast, treatment with MG132 alone reduced the expression of PSMA7, but not the core protein (Figure 3C), whereas expression of NS3 was reduced by treatment with 17-AAG or MG132 alone, and 17-AAG plus MG132. This result was consistent with our previous findings that NS3 levels were reduced in NNC#2 cells treated with 17-AAG for 3 days, but that core protein

Table 1. Combination index and dose reduction in inhibition of hepatitis C virus RNA replication by combining 17-AAG with MG132

Drug	IC_{50}, nM		Fold dose reduction[a]
	Alone	In combination	
17-AAG	0.82	0.33	2.52
MG132	0.21	0.01	21.00

The combination index for 17-AAG and MG132 was 0.42. [a]Dose reduction is the 50% inhibitory concentration (IC_{50}) of the drug in combination. Each sample was tested in triplicate and the mean values are presented

was detected for up to 6 days [15]. Other researchers, however, have reported that MG132 blocks the degradation of HCV core protein [31]. Interestingly, combined treatment with MG132 and 17-AAG reduced the expression of both the core and PSMA7 proteins in NNC#2 cells (Figure 3C). These results suggest that MG132 and 17-AAG are potent anti-HCV agents, and are more effective in combination therapy than as single monotherapeutic agents.

Discussion

HCV is a major cause of chronic liver disease. The results of the present study indicate that the individual effects of the Hsp90 inhibitor 17-AAG on HCV replicon cells and the synergistic action of the proteasome inhibitor MG132 might account for the improved clinical response to combination therapy. We previously reported a new and effective strategy for inhibiting HCV replication using 17-AAG to inhibit Hsp90 [15]. The mechanism by which 17-AAG so effectively suppresses HCV replication is the destabilization of NS3, which disrupts the Hsp90 chaperone complex. A previous study demonstrated that HCV NS3 degradation is greatly increased by treatment of HCV subgenomic replicon #50-1 cells with 17-AAG, but this degradation is completely blocked in the presence of the proteasome inhibitor MG132 [15]. By contrast, in the present study we used HCV full-length replicon NNC#2 cells in place of HCV subgenomic replicon #50-1 cells used in previous studies [15]. The resulting 17-AAG treatment reduced NS3 levels, but MG132 treatment of NNC#2 cells did not block the degradation of HCV NS3 (Figure 1D). This blocking efficiency significantly influenced the different activities of the virus IRES (that is, HCV IRES and EMCV IRES) [25–28]. In our assays, when Huh-7 cells exposed to MG132 were transfected with pHCV IRES luc or pEMCV IRES luc, HCV IRES activity was inhibited, but EMCV IRES was not (Figure 2B). Apcher *et al.* [29] reported that HCV IRES-mediated translation can be induced by PSMA7. The proteasome inhibitor MG132 inhibits PSMA7 activity. These findings demonstrate that HCV IRES activity is also reduced by MG132. By contrast, degradation of NS3 by 17-AAG is dependent on the proteasome system [15].

The present study demonstrated that NNC#2 cells containing a full HCV genome replicon treated with 17-AAG or MG132 for 3 days did not show dose-dependent cytotoxicity (Figure 3A), but 10 μM MG132 was cytotoxic (data not shown). As shown in the present study, the IC_{50} values were 0.82 nM for 17-AAG and 0.21 nM for MG132 (Table 1 and Figure 3B). These data provide evidence that a dual treatment strategy with 17-AAG and MG132 inhibits HCV replication. The combination of 5 nM 17-AAG and 1 nM MG132 suppressed HCV RNA replication by 90% in NNC#2 HCV replicon cells (Figure 3B). The two drugs, 17-AAG and MG132, had synergistic inhibitory effects on HCV replicon (Table 1). Importantly, the combined use of these different groups of inhibitors showed strong synergistic inhibitory effects on HCV replication, indicating that combining these inhibitors might be a useful and efficient strategy for anti-HCV chemotherapy.

Given the absence of a single effective and proven antiviral agent against HCV, the combination of 17-AAG with agents that possess potential antiviral effects will continue to dominate novel therapeutic approaches. The present study demonstrated a strong synergistic effect of 17-AAG and MG132 on intracellular HCV replication, and these effects are attributable to the direct and specific inhibition of viral replication. Our results indicate that antiviral treatment with 17-AAG might be improved by combining 17-AAG with MG132, and that this combination therapy might be a feasible strategy for the treatment of HCV infection. Modifications of these inhibitors might also result in the development of more effective antiviral compounds.

Acknowledgements

We are grateful to M Sato and Y Katumura for excellent technical assistance. This work was supported by a Grant-in-Aid for HCV research from the Ministry of Health, Labor, and Welfare of Japan, and by a Grant-in-Aid for High Technology Research from the Ministry of Education, Science, Sports, and Culture of Japan.

Disclosure statement

The authors declare no competing interests.

References

1. Alter HJ, Purcell RH, Shin JW, *et al.* Detection of antibody to hepatitis C virus in prospectively followed transfusion recipients with acute and chronic non-A, non-B hepatitis. *N Engl J Med* 1989; 321:1494–1500.
2. Choo QL, Kuo G, Weiner AJ, Overby LR, Bradley DW, Houghton M. Isolation of a cDNA clone derived from a blood-borne non-A, non-B viral hepatitis genome. *Science* 1989; 244:359–362.
3. Chevaliez S, Pawlotsky JM. Hepatitis C virus: virology, diagnosis and management of antiviral therapy. *World J Gastroenterol* 2007; 13:2461–2466.
4. Witthöft T. Review of consensus interferon in the treatment of chronic hepatitis C. *Biologics* 2008; 2:635–643.
5. Saito I, Miyamuram T, Ohbayashi A, *et al.* Hepatitis C virus infection is associated with the development of hepatocellular carcinoma. *Proc Natl Acad Sci U S A* 1990; 87:6547–6549.

6. Seeff LB. Natural history of hepatitis C. *Hepatology* 1997; 26:21S–28S.
7. Reddy KR, Wright TL, Pockros PJ, *et al.* Efficacy and safety of pegylated (40-kd) interferon alpha-2a compared with interferon alpha-2a in noncirrhotic patients with chronic hepatitis C. *Hepatology* 2001; 33:433–438.
8. McClellan AJ, Frydaman J. Molecular chaperones and the art of recognizing a lost cause. *Nat Cell Biol* 2001; 3:E51–E53.
9. Pratt WB, Toft DO. Regulation of signalling protein function and trafficking by the hsp90/hsp70-based chaperone machinery. *Exp Biol Med (Maywood)* 2003; 228:111–133.
10. Picard D. Heat-shock protein 90, a chaperone for folding and regulation. *Cell Mol Life Sci* 2002; 59:1640–1648.
11. Wegele H, Muller L, Buchner J. Hsp70 and Hsp90–α relay team for protein folding. *Rev Physiol Biochem Pharmacol* 2004; 151:1–44.
12. Basso AD, Solit DB, Munster PN, Rosen N. Ansamycin antibiotics inhibit Akt activation and cyclin D expression in breast cancer cells that overexpress HER2. *Oncogene* 2002; 21:1159–1166.
13. Kelland LR, Sharp SY, Rogers PM, Myers TG, Workman P. DT-diaphorase expression and tumor cell sensitivity to 17-allylamino, 17-demethoxygeldanamycin, an inhibitor of heat shock protein 90. *J Natl Cancer Inst* 1999; 91:1940–1949.
14. Solit DB, Zheng FF, Drobnjak M, *et al.* 17-allylamino-17-demthoxygeldanamycin induces the degradation of androgen receptor and HER-2/neu and inhibits the growth of prostate cancer xenografts. *Clin Cancer Res* 2002; 8:986–993.
15. Ujino S, Yamaguchi S, Shimotohno K, Takaku H. Heat-shock protein 90 is essential for stabilization of the hepatitis C virus nonstructural protein NS3. *J Biol Chem* 2009; 284:6841–6846.
16. Supko JG, Hickman RL, Grever MR, Malspeis L. Preclinical pharmacologic evaluation of geldanamycin as an antitumor agent. *Cancer Chemother Pharmacol* 1995; 36:305–315.
17. Grenert JP, Sullivan WP, Fadden P, *et al.* The amino-terminal domain of heat shock protein 90 (hsp90) that binds geldanamycin is an ATP/ADP switch domain that regulates hsp90 conformation. *J Biol Chem* 1997; 272:23843–23850.
18. Tanaka K. Molecular biology of the proteasome. *Biochem Biophys Res Commun* 1998; 247:537–541.
19. Krüger M, Beger C, Welch PJ, Barber JR, Manns MP, Wong-Staal F. Involvement of proteasome α-subunit PSMA7 in hepatitis C virus internal ribosome entry site-mediated translation. *Mol Cell Biol* 2001; 21:8357–8364.
20. Korf M, Jarczak D, Beger C, Manns MP, Krüger M. Inbibition of hepatitis C virus translation and subgenomic replication by siRNAs directed against highly conserved HCV sequence and cellular HCV cofactors. *J Hepatol* 2005; 43:225–234.
21. Ishii N, Watashi K, Hishiki T, *et al.* Diverse effects of cyclosporine on hepatitis C virus strain replication. *J Virol* 2006; 80:4510–4520.
22. Kishine H, Sugiyama K, Hijikata M, *et al.* Subgenomic replicon derived from a cell line infected with the hepatitis C virus. *Biochem Biophys Res Commun* 2002; 293:993–999.
23. Takeuchi T, Katsume A, Tanaka T, *et al.* Real-time detection system for quantification of hepatitis C virus genome. *Gastroenterology* 1999; 116:636–642.
24. Tanabe Y, Sakamoto N, Enomoto N, *et al.* Synergistic inhibition of intracellular hepatitis C virus replication by combination of ribavirin and interferon-α. *J Infect Dis* 2004; 189:1129–1139.
25. Tsukiyama-Kohara K, Iizuka N, Kohara M, Nomoto A. Internal ribosome entry site within hepatitis C virus RNA. *J Virol* 1992; 66:1476–1483.
26. Hellen CU, Pestova TV. Translation of hepatitis C virus RNA. *J Viral Hepat* 1999; 6:79–87.
27. Honda M, Beard MR, Ping LH, Lemon SM. A phylogenetically conserved stem-loop structure at the 5′ border of the internal ribosome entry site of hepatitis C virus is required for cap-independent viral translation. *J Virol* 1999; 73:1165–1174.
28. Hellen CU, Wimmer E. Translation of encephalomycarditis virus RNA by internal ribosomal entry. *Curr Top Microbiol Immunol* 1995; 203:31–63.
29. Apcher GS, Maitland J, Dawson S, Sheppard P, Mayer RJ. The alpha4 and alpha7 subunits and assembly of the 20S proteasome. *FEBS Lett* 2004; 569:211–216.
30. Meiners S, Heyken D, Weller A, *et al.* Inhibition of proteasome activity induces concerted expression of proteasome genes and *de novo* formation of mammalian proteasomes. *J Biol Chem* 2003; 278:21517–21525.
31. Moriishi K, Okabayashi T, Nakai K, *et al.* Proteasome activator PA28gamma-dependent nuclear retention and degradation of hepatitis C virus core protein. *J Virol* 2003; 77:10237–10249.

Received 27 July 2009, accepted 19 September 2009

Journal of
Medicinal
Chemistry
Brief Article

J. Med. Chem. **XXXX,** *XXX,* 000–000 A
DOI: 10.1021/jm1003528

Peptide HIV-1 Integrase Inhibitors from HIV-1 Gene Products

Shintaro Suzuki,[†,#] Emiko Urano,[‡,#] Chie Hashimoto,[†] Hiroshi Tsutsumi,[†] Toru Nakahara,[†] Tomohiro Tanaka,[†] Yuta Nakanishi,[†] Kasthuraiah Maddali,[§] Yan Han,[‡] Makiko Hamatake,[‡] Kosuke Miyauchi,[‡] Yves Pommier,[§] John A. Beutler,[⊥] Wataru Sugiura,[‡] Hideyoshi Fuji,[∥] Tyuji Hoshino,[∥] Kyoko Itotani,[†] Wataru Nomura,[†] Tetsuo Narumi,[†] Naoki Yamamoto,[‡] Jun A. Komano,[‡] and Hirokazu Tamamura*[,†]

[†]*Department of Medicinal Chemistry, Institute of Biomaterials and Bioengineering, Tokyo Medical and Dental University, 2-3-10 Kandasurugadai, Chiyoda-ku, Tokyo 101-0062, Japan,* [‡]*AIDS Research Center, National Institute of Infectious Diseases, 1-23-1 Toyama, Shinjuku-ku, Tokyo 162-8640, Japan,* [§]*Laboratory of Molecular Pharmacology, Center for Cancer Research, National Cancer Institute, National Institutes of Health, Bethesda, Maryland 20892-4255,* [∥]*Department of Physical Chemistry, Graduate School of Pharmaceutical Sciences, Chiba University, 1-33 Yayoi-cho, Inage-ku, Chiba 263-8522, Japan, and* [⊥]*Molecular Targets Laboratory, Center for Cancer Research, National Cancer Institute, National Institutes of Health, Frederick, Maryland 21702.* [#] *These authors contributed equally to this work.*

Received March 17, 2010

Anti-HIV peptides with inhibitory activity against HIV-1 integrase (IN) have been found in overlapping peptide libraries derived from HIV-1 gene products. In a strand transfer assay using IN, inhibitory active peptides with certain sequential motifs related to Vpr- and Env-derived peptides were found. The addition of an octa-arginyl group to the inhibitory peptides caused a remarkable inhibition of the strand transfer and 3′-end-processing reactions catalyzed by IN and significant inhibition against HIV replication.

Introduction

Many antiretroviral drugs are currently available to treat human immunodeficiency virus type 1 (HIV-1) infection. Viral enzymes such as reverse transcriptase (RT[a]), protease and integrase (IN), gp41, and coreceptors are the main targets for antiretroviral drugs that are under development. Because of the emergence of viral strains with multidrug resistance (MDR), however, new anti-HIV-1 drugs operating with different inhibitory mechanisms are required. Following the success of raltegravir, IN has emerged as a prime target. IN is an essential enzyme for the stable infection of host cells because it catalyzes the insertion of viral DNA inside the preintegration complex (PIC) into the genome of host cells in two successive reactions, designated as strand transfer and 3′-end-processing. It is assumed that the enzymatic activities of IN have to be negatively regulated in the PIC during its transfer from the cytoplasm to the nucleus. Otherwise, premature activation of IN can lead to the autointegration into the viral DNA itself, resulting in an aborted infection. We speculate that the virus, rather than the host cells, must encode a mechanism to prevent autointegration. The PIC contains in association with the viral nucleic acid, viral proteins such as RT, IN, capsids ($p24^{CA}$ and $p7^{NC}$), matrix ($p17^{MA}$), p6 and Vpr, cellular proteins HMG I (Y), and the barrier to autointegration factor (BAF).[1−4] It is likely that, due to their spatial proximity in the PIC, these proteins physically and functionally interact with each other. For instance, it is already known that RT activity inhibited by Vpr,[5] and that RT and IN inhibit each other.[5−9] Vpr also inhibits IN through its C-terminal domain.[5,10] Because these studies suggest that PIC components regulate each other's function, we have attempted to obtain potent inhibitory lead compounds from a peptide fragment library derived from HIV-1 gene products, an approach which has been successful in finding a peptide IN inhibitor from LEDGF, a cellular IN binding protein.[11]

In this paper, we describe the screening of an overlapping peptide library derived from HIV-1 proteins, the identification of certain peptide motifs with inhibitory activity against HIV-1 IN, and the evaluation of effective inhibition of HIV-1 replication in cells using the identified peptide inhibitors possessing cell membrane permeability.

Results and Discussion

An overlapping peptide library spanning HIV-1 SF2 *Gag*, *Pol*, *Vpr*, *Tat*, *Rev*, *Vpu*, *Env*, and *Nef*, provided by Dr. Iwamoto of the Institute of Medical Science at the University of Tokyo (Supporting Information, SI, Figure 2A), was screened with a strand transfer assay[12] in search of peptide pools with inhibitory activity against HIV-1 IN. The library consists of 658 peptide fragments derived from the HIV-1 gene products. Each peptide is composed of 10−17 amino acid residues with overlapping regions of 1−7 amino acid residues. Sixteen peptide pools containing between 16 and 65 peptides were used for the first screening at the final concentration of 5.0 μM for each peptide (SI Figure 2B). This initial screening gave the results shown in Figure 1. Both Vpr and Env4 pools showed remarkable inhibition of IN strand transfer activity, and consequently a second screening was performed using the individual peptides contained in the Vpr and Env4 pools. A group of consecutive overlapping peptides in the Vpr pool (groups 13−15) and groups 4−6 and 20−21 in the Env4 pool were found to possess IN inhibitory activity (Figure 2). We focused on Vpr15 and Env4-4 peptides because they showed inhibitory activity against IN strand transfer reaction in a dose-dependent manner (Figure 3). The IC_{50} values of Vpr15

*To whom correspondence should be addressed. Phone: +81-3-5280-8036. Fax: +81-3-5280-8039. E-mail: tamamura.mr@tmd.ac.jp.

[a]Abbreviations: HIV, human immunodeficiency virus; IN, integrase; RT, reverse transcriptase; MDR, multidrug resistance; PIC, preintegration complex; BAF, barrier to autointegration factor; R_8, octa-arginyl.

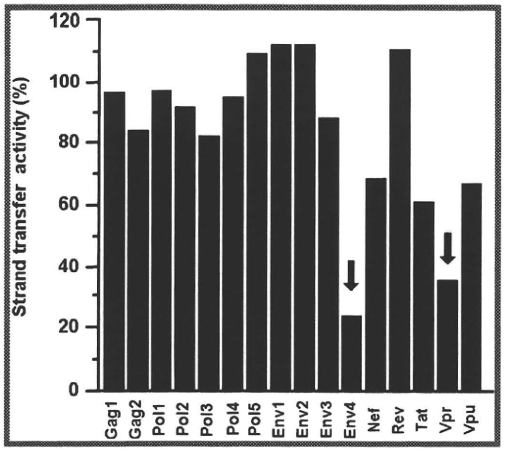

Figure 1. Inhibition of the IN strand transfer activity by peptide pools. Inhibition of the IN strand transfer activity was strongly inhibited by Env4 and Vpr pools (arrows). The *y*-axis represents the IN strand transfer activity relative to the solvent control (DMSO).

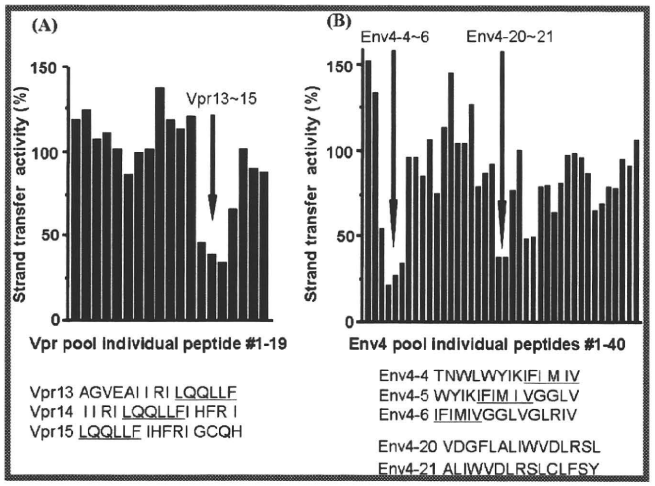

Figure 2. Identification of IN inhibitory peptides in the Vpr (A) and Env4 (B) pools based on the strand transfer activity of IN. The consecutive overlapping peptides display the inhibition of the strand transfer activity of IN (arrows). The *y*-axis represents the IN strand transfer activity relative to the solvent control (DMSO). The concentration of each peptide was 5 μM. The common sequences of individual peptides derived from Vpr and Env4 pools with anti-IN activity are underlined.

and Env4-4 were estimated at 5.5 and 1.9 μM, respectively. These peptides did not show any significant inhibitory activity against HIV-1 RT, suggesting that they might inhibit IN strand transfer reaction selectively.

The overlapping peptides of Vpr13-15 and Env4-4-6 have the vommon hexapeptide sequences LQQLLF and IFIMIV, respectively. The LQQLLF sequence covers positions 64−69 of Vpr, which is a part of the second helix of Vpr. The IFIMIV sequence corresponds to positions 684−689 of gp160, which is a part of the transmembrane domain of TM/gp41. These hexapeptides are thought to be critical to inhibition of IN activity. It was recently reported[5] that similar peptides derived from Vpr inhibit IN with IC_{50} values of 1−16 μM, which is consistent with our data. In this report,[5] the peptide motif was found to be 15 amino acid residues spanning LQQLLF from the overlapping Vpr peptide library. In our study, more precise mapping of inhibitory motif in Vpr peptides was achieved by identifying the shorter effective peptide motif. We focused on the Vpr-derived peptide, LQQLLF (Vpr-1) to develop potent inhibitory peptides. However, the expression of inhibitory activity against IN

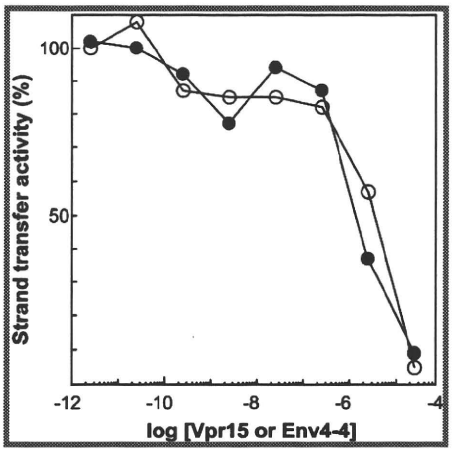

Figure 3. Concentration-dependent inhibition of IN strand transfer activities by Vpr15 (○) and Env4−4 (●) peptides. The *y*-axis represents the IN strand transfer activity relative to the solvent control (DMSO).

in vivo by only hexapeptides might be difficult because these hexapeptides penetrate the plasma membrane very poorly and to achieve antiviral activity, it is essential that they penetrate the cell membrane. To that effect, an octa-arginyl (R_8) group[13] was fused to the Vpr-derived peptides (Table 1). R_8 is a cell membrane permeable motif and its fusion with parent peptides successfully generates bioactive peptides without significant adverse effects or cytotoxicity.[14−18] In addition, the R_8-fusion could increase the solubility of Vpr-derived peptides which have a relatively hydrophobic character.

The inhibitory activity of Vpr-1 and Vpr-1-4 R_8 peptides against IN was evaluated based on the strand transfer and 3′-end-processing reactions in vitro (Table 1).[19,20] Vpr-1 did not show strong inhibition of either IN activity, but the IC_{50} of Vpr-1 R_8 toward the strand transfer reaction of IN was 10-fold lower than that of Vpr-1 lacking the R_8 group. This indicates that the positive charges derived from the R_8 group might enhance the inhibitory activity of the Vpr-1 peptide. Because we were concerned that the strong positive charges close to the LQQLLF motif might interfere with the inhibitory activity, the 6 amino acid sequence (−IHFRIG−) was inserted as a spacer between LQQLLF and R_8 (Vpr-3 R_8). The IHFRIG sequence was used to reconstitute the natural Vpr. The IC_{50} values of Vpr-2 R_8 for the strand transfer and 3′-end-processing activities of IN were 0.70 and 0.83 μM, respectively, while Vpr-3 R_8 showed potent IN inhibitory activities of 4.0 and 8.0 nM against the strand transfer and 3′-end- processing activities, respectively. This result indicates the additional importance of the IHFRIG sequence for inhibitory activities against IN. The increased IN inhibitory activities might be achieved presumably by the synergistic effect of the LQQLLF motif, the IHFRIG sequence, and the R_8 group. Vpr-4 R_8, in which the EAIIRI sequence was attached to further reconstitute the Vpr helix 2, showed inhibitory activities similar to those of Vpr-3 R_8, suggesting that reconstitution of helix 2 of Vpr is not necessary for efficient IN inhibition. Vpr-3 R_8 and Vpr-4 R_8, with $IC_{50} > 0.5\,\mu$M,[21] were less potent inhibitors of RT-associated RNase H activity, indicating that these peptides can selectively inhibit IN. These results suggest that Vpr-derived peptides are novel and distinct from any other IN inhibitors reported to date.

For rapid assessment of the antiviral effect of Vpr-derived peptides, we established an MT-4 Luc system in which MT-4 cells were stably transduced with the firefly luciferase expression cassette by a murine leukemia viral vector (SI Figure 3).

Table 1. Sequences of Vpr-Derived Peptides and Their IC_{50} Values toward the Strand Transfer and 3′-End Processing Reactions of IN

	sequence	IC_{50} (μM) strand transfer	IC_{50} (μM) 3′-end processing
Vpr-1	LQQLLF	68 ± 1.0	>100
Vpr-1 R_8	Ac-LQQLLF -RRRRRRRR-NH_2	6.1 ± 1.1	>11
Vpr-2 R_8	Ac-IHFRIG-RRRRRRRR-NH_2	0.70 ± 0.06	0.83 ± 0.07
Vpr-3 R_8	Ac-LQQLLF IHFRIG-RRRRRRRR-NH_2	0.004 ± 0.0001	0.008 ± 0.001
Vpr-4 R_8	Ac-EAIIRI LQQLLF IHFRIG-RRRRRRRR-NH_2	0.005 ± 0.002	0.006 ± 0.006

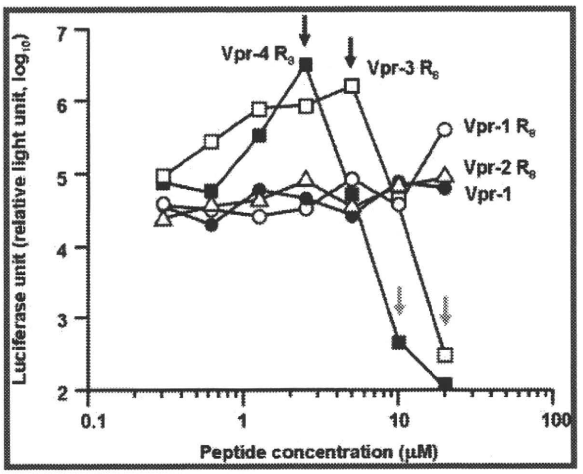

Figure 4. Luciferase signals in MT-4 Luc cells infected with HIV-1 in the presence of various concentrations of Vpr-derived peptides: Vpr-1 (●), Vpr-1 R_8 (○), Vpr-2 R_8 (△), Vpr-3 R_8 (□), Vpr-4 R_8 (■).

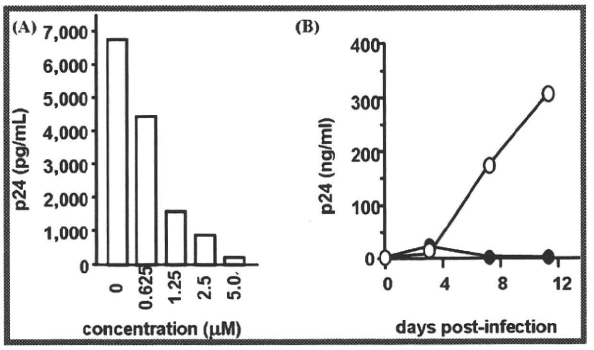

Figure 5. (A) The inhibition of HIV-$1_{JR\text{-}CSF}$ replication in NP2-CD4-CCR5 cells in the presence of various concentrations of Vpr-3 R_8. (B) The replication kinetics of HIV-1_{HXB2} in MT-4 cells in the presence of Vpr-3 R_8 (●). The concentration of Vpr-3 R_8 was fixed at 0.5 μM. Absence of Vpr-3 R_8 (○).

MT-4 Luc cells constitutively express high levels of luciferase which are significantly reduced by HIV-1 infection due to their high susceptibility to cell death upon HIV-1 infection. Protection of MT-4 Luc cells from HIV-1-induced cell death maintains the luciferase signals at high levels. In addition, the cytotoxicity of Vpr-derived peptides can be evaluated by a decrease of luciferase signals in these MT-4 Luc systems. Vpr-2 R_8, which is a weak IN inhibitor, showed no significant anti-HIV-1 activity below concentrations of 20 μM, suggesting that its moderate IC_{50} level in vitro is not sufficient to suppress HIV-1 replication in tissue culture and that the R_8 group is not significantly cytotoxic (Figure 4). Vpr-1 did not show any inhibitory effects against HIV-1 replication; however, Vpr-1 R_8 displayed a weak antiviral effect at a concentration of 20 μM and both Vpr-3 R_8 and Vpr-4 R_8 showed significant inhibitory effects against HIV-1 replication. The R_8 peptide did not show significant anti-HIV activity (IC_{50} > 50 μM, data not shown). These results suggest that the addition of the R_8 group enables Vpr-derived peptides to enter the cytoplasm and access IN, with the result that HIV-1 replication could be effectively inhibited.

Because Vpr-3 R_8 was less cytotoxic than Vpr-4 R_8, the inhibitory activities of Vpr-3 R_8 were further investigated. Two replication assay systems, R5-tropic HIV-$1_{JR\text{-}CSF}$ on NP2-CD4-CCR5 cells and X4-tropic HIV-1_{HXB2} on MT-4 cells, were utilized. NP2-CD4-CCR5 cells were infected with HIV-$1_{JR\text{-}CSF}$ in the presence of various concentrations of Vpr-3 R_8. On day 4 postinfection, the culture supernatant was collected and the concentration of viral p24 antigen was measured by an ELISA assay. The p24 levels decreased in a dose-dependent manner with increasing the concentration of Vpr-3 R_8; 50% inhibition of p24 expression was obtained with approximately 0.8 μM of Vpr-3 R_8 (Figure 5A). This concentration was approximately 10-fold lower than the concentration of Vpr-3 R_8 known to be cytotoxic (Figure 4). Second, MT-4 cells were infected with HIV-1_{HXB2} and the replication kinetics was monitored in the presence of 0.5 μM Vpr-3 R_8. The degree of replication of HIV-1_{HXB2} was quite low in the presence of Vpr-3 R_8, while replication of HIV-1_{HXB2} was robust in the absence of Vpr-3 R_8 (Figure 5B), suggesting that Vpr-3 R_8 strongly suppresses the replication of HIV-1 in cells. To examine whether the HIV-1 replication was blocked through the inhibition of IN activity, quantitative real-time PCR was performed. If IN is inhibited, the efficiency of viral genome integration should be decreased while the reverse transcription of viral genome should not be affected. Accordingly, NP2-CD4-CXCR4 cells were infected with HIV-1_{HXB2} in the presence or absence of 0.5 μM Vpr-3 R_8. Genomic DNA was extracted on day 2 postinfection, and the viral DNA was quantified at the various steps of viral entry phase. The level of "strong stop DNA", representing the total genome of infected virus in Vpr-3 R_8-treated cells, was similar (139.7%) to that in DMSO-treated control cells and the level of viral DNA generated at the late stage of reverse transcription in Vpr-3 R_8-treated cells was slightly decreased (84.4%) compared to control cells. This small decline can probably be attributed to the weak anti-RNase H activity of Vpr-3 R_8. On the other hand, a drastic decrease of Alu-LTR products was observed in Vpr-3 R_8-treated cells (15.8%), indicating an inhibition of integrated viral genome. Concomitantly, the double LTR products, representing the end-joined viral genome catalyzed by host cellular enzymes, were increased by a factor of 8 (779.8%). These results strongly suggest that Vpr-3 R_8 blocks viral infection by inhibiting IN activity in cells, consistent with our in vitro observations. Judging by these results, Vpr-derived peptides with the R_8 group are potent IN inhibitors that suppress HIV-1 replication in vivo.

Finally, in silico molecular docking simulations of Vpr-derived peptides and HIV-1 IN were performed. The Vpr-derived peptides are located in the second helix of Vpr and were thus considered to have an α-helical conformation.[22] Docking simulations of three peptides (Vpr13, Vpr14, and Vpr15), using the predicted structure of the HIV-1 IN dimer as a template,[23] were performed by GOLD software to investigate the binding mode of the peptides, the binding affinity of

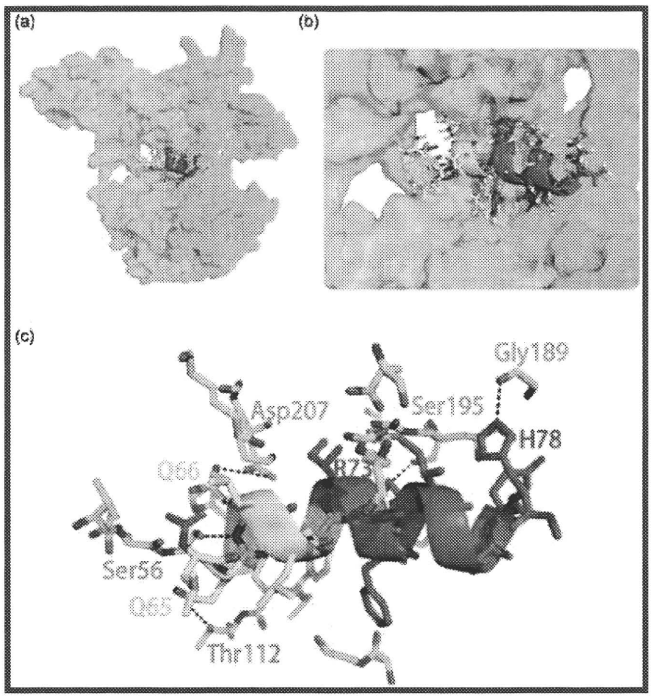

Figure 6. Predicted binding mode of Vpr15 to HIV-1 IN by GOLD. An overall view of (a) the complex obtained by docking Vpr15 with the HIV-1 IN dimer and (b) the closer view of the complex. The predicted structure of full-length HIV-1 IN was used as a template. Each HIV-1 IN monomer was shown as green or cyan surface. The docked Vpr15 is shown as a cartoon. The yellow-colored region is the LQQLLF motif. The GOLD score representing the docking complementarity is 69.83, indicating the high binding affinity between Vpr15 and IN. The hydrogen-bond interactions between HIV-1 IN and Vpr15 were presented by LIGPLOT software shown as blue dotted line (c).

the peptides being evaluated by GOLD Fitness score. The predicted binding mode of Vpr15 to IN is shown in Figure 6. Our results predict that the three Vpr-derived peptides interact with the cleft between the amino-terminal domain and the core domain of HIV-1 IN. This region is distinct from the nucleic acid interacting surfaces, indicating that the Vpr-derived peptides inhibit IN function in an allosteric manner. A previous report provided a model in which a Vpr peptide was bound to IN in a manner similar with our model[5] and, interestingly, the peptides were bound to IN with an exterior surface of Vpr. This earlier report that the full-length Vpr inhibits IN[10] strongly supports the predicted binding mode of Vpr15. Five hydrogen-bond interactions between HIV-1 IN and Vpr15 were identified by LIGPLOT analysis,[24] which invoked the following IN-Vpr amino acids: IN Thr112-Vpr Gln65, IN Ser56-Vpr Gln66, IN Asp207-Vpr Gln66, IN Ser195-Vpr Arg73, and IN Gly189-Vpr His78. The numbering of Vpr amino acids is based on the Vpr full-length coordinate, Figure 6. Additional hydrophobic contacts between IN and Vpr15 were found in which the following IN-Vpr amino acid pairs are involved: IN Lys211-Vpr Gln66, IN Pro109-Vpr Phe69, IN Arg262-Vpr His71, and IN Arg187-Vpr Gln77. These data indicate that the Gln65, Gln66, and Phe69 residues in Vpr-derived peptides play a major role in the interaction between IN and Vpr-derived peptides.

Conclusions

In summary, two peptide motifs, LQQLLF from Vpr and IFIMIV from Env4, possessing inhibitory activity against HIV-1 IN, were identified through the screening of overlapping peptide library derived from HIV-1 gene products. We initially speculate that HIV encodes a mechanism to prevent autointegration in the PIC because integration activity must be regulated until the virus infects cells. This speculation is supported by the finding that IN inhibitors exist in the viral PIC components. Vpr-derived peptides with the R_8 group showed remarkable inhibitory activities against the strand transfer and 3′-end-processing reactions catalyzed by HIV-1 IN in vitro. In addition, Vpr-3 R_8 and Vpr-4 R_8 were shown to inhibit HIV-1 replication with submicromolar IC_{50} values in cells using the MT-4 Luc cell system. In the quantitative analysis of p24 antigen, 50% inhibition of HIV-$1_{JR\text{-}CSF}$ replication was caused by approximately 0.8 μM of Vpr-3 R_8, and the replication of HIV-1_{HXB2} was extensively suppressed in the long term by Vpr-3 R_8 at 0.5 μM concentrations. Our finding suggest that these peptides could serve as lead compounds for novel IN inhibitors. Amino acid residues critical to the interaction of Vpr-derived peptides with IN were identified by our in silico molecular docking simulations, and suggests that more potent peptides[25] or peptidomimetic IN inhibitors represent a novel avenue for future small molecule inhibitors of IN and HIV integration.

Experimental Section

Peptide Synthesis. Vpr-derived peptides containing the R_8 group were synthesized by stepwise elongation techniques of Fmoc-protected amino acids on NovaSyn TGR resin. Coupling reactions were performed using 5.0 equiv of Fmoc-protected amino acid, 5.0 equiv of diisopropylcarbodiimide, and 5.0 equiv of 1-hydroxybenzotriazole monohydrate. Cleavage of peptides from resin and side chain deprotection were carried out with 10 mL of TFA in the presence of 0.25 mL of *m*-cresol, 0.75 mL of thioanisole, 0.75 mL of 1,2-ethanedithiol, and 0.1 mL of water as scavenger by stirring for 1.5 h. After filtration of the deprotected peptides, the filtrate was concentrated under reduced pressure, and crude peptides were precipitated in cooled diethylether. All crude peptides were purified by RP-HPLC and identified by MALDI-TOFMS. Purities of all final compounds were confirmed (>95% purity) by analytical HPLC. Detailed data are provided in SI.

Enzyme Assays. The strand transfer assay for the first screening was performed as described previously.[12] The IN strand transfer and 3′-end-processing assays for peptide motif characterizations were performed as described previously.[19,20] RNase H activity was measured as described by Beutler et al.[21]

Replication Assays. For HIV-1 replication assays, 1×10^5 cells were incubated at room temperature for 30 min with an HIV-1 containing culture supernatant (ca. 0.2−50 ng p24) and then washed and incubated. Culture supernatants were collected at different time points, and then the cells were passaged if necessary. Levels of p24 antigen were measured using a Retro TEK p24 antigen ELISA kit, according to the manufacture's protocol. Signals were detected using an ELx808 microplate photometer.

For MT-4 Luc assays, MT-4 Luc cells (1×10^3 cells) grown in 96-well plates were infected with HIV-1_{XHB2} (ca. 0.2−10 ng p24) in the presence of varying concentrations of Vpr-3 R_8. At 6−7 d postinfection, cells were lysed and luciferase activity was measured using the Steady-Glo assay kits according to the manufacture's protocol. Chemiluminescence was detected with a Veritas luminometer.

Acknowledgment. We thank Prof. A. Iwamoto's group of the Institute of Medical Science at the University of Tokyo for the peptide libraries and Dr. M. Nicklaus from NCI/NIH for providing the modeled structure of full-length HIV-1 IN. T.T. is supported by JSPS research fellowships for young scientists.

This work was supported in part by Grant-in-Aid for Scientific Research from the Ministry of Education, Culture, Sports, Science, and Technology of Japan, and Health and Labor Sciences Research Grants from Japanese Ministry of Health, Labor, and Welfare. K.M. and Y.P. are supported by the Intramural Program of the National Cancer Institute, Center for Cancer Research.

Supporting Information Available: Additional experimental procedures including MS data and figures; HPLC charts of final compounds, explanation for HIV-1 genes and the peptide pools, and illustration of MT-4 Luc system. This material is available free of charge via the Internet at http://pubs.acs.org.

References

(1) Bukrinsky, M. I.; Haggerty, S.; Dempsey, M. P.; Sharova, N.; Adzhubei, A.; Spitz, L.; Lewis, P.; Goldfarb, D.; Emerman, M.; Stevenson, M. A nuclear-localization signal within HIV-1 matrix protein that governs infection of nondividing cells. *Nature* **1993**, *365*, 666–669.

(2) Miller, M. D.; Farnet, C. M.; Bushman, F. D. Human immunodeficiency virus type 1 preintegration complexes: studies of organization and composition. *J. Virol.* **1997**, *71*, 5382–5390.

(3) Farnet, C. M.; Bushman, F. D. HIV-1 cDNA integration: Requirement of HMG I(Y) protein for function of preintegration complexes in vitro. *Cell* **1997**, *88*, 483–492.

(4) Chen, H.; Engelman, A. The barrier-to-autointegration protein is a host factor for HIV type 1 integration. *Proc. Natl. Acad. Sci. U.S.A.* **1998**, *95*, 15270–15274.

(5) Gleenberg, I. O.; Herschhorn, A.; Hizi, A. Inhibition of the activities of reverse transcriptase and integrase of human immunodeficiency virus type-1 by peptides derived from the homologous viral protein R (Vpr). *J. Mol. Biol.* **2007**, *369*, 1230–1243.

(6) Gleenberg, I. O.; Avidan, O.; Goldgur, Y.; Herschhorn, A.; Hizi, A. Peptides derived from the reverse transcriptase of human immunodeficiency virus type 1 as novel inhibitors of the viral integrase. *J. Biol. Chem.* **2005**, *280*, 21987–21996.

(7) Hehl, E. A.; Joshi, P.; Kalpana, G. V.; Prasad, V. R. Interaction between human immunodeficiency virus type I reverse transcriptase and integrase proteins. *J. Virol.* **2004**, *78*, 5056–5067.

(8) Tasara, T.; Maga, G.; Hottiger, M. O.; Hubscher, U. HIV-1 reverse transcriptase and integrase enzymes physically interact and inhibit each other. *FEBS Lett.* **2001**, *507*, 39–44.

(9) Gleenberg, I. O.; Herschhorn, A.; Goldgur, Y.; Hizi, A. Inhibition of human immunodeficiency virus type-1 reverse transcriptase by a novel peptide derived from the viral integrase. *Arch. Biochem. Biophys.* **2007**, *458*, 202–212.

(10) Bischerour, J.; Tauc, P.; Leh, H.; De Rocquigny, H.; Roques, B.; Mouscadet, J. F. The (52−96) C-Terminal domain of Vpr stimulates HIV-1 IN-mediated homologous strand transfer of mini-viral DNA. *Nucleic Acids Res.* **2003**, *31*, 2694–2702.

(11) Hayouka, Z.; Rosenbluh, J.; Levin, A.; Loya, S.; Lebendiker, M.; Veprintsev, D.; Kotler, M.; Hizi, A.; Loyter, A.; Friedler, A. Inhibiting HIV-1 integrase by shifting its oligomerization equilibrium. *Proc. Natl. Acad. Sci. U.S.A.* **2007**, *104*, 8316–8312.

(12) Yan, H.; Mizutani, T. C.; Nomura, N.; Tanaka, T.; Kitamura, Y.; Miura, H.; Nishizawa, M.; Tatsumi, M.; Yamamoto, N.; Sugiura, W. A novel small molecular weight compound with a carbazole structure that demonstrates potent human immunodeficiency virus type-1 integrase inhibitory activity. *Antivir. Chem. Chemother.* **2005**, *16*, 363–373.

(13) Suzuki, T.; Futaki, S.; Niwa, M.; Tanaka, S.; Ueda, K.; Sugiura, Y. Possible existence of common internalization mechanisms among arginine-rich peptides. *J. Biol. Chem.* **2002**, *277*, 2437–2443.

(14) Wender, P. A.; Mitchell, D. J.; Pattabiraman, K.; Pelkey, E. T.; Steinman, L.; Rothbard, J. B. The design, synthesis, and evaluation of molecules that enable or enhance cellular uptake: Peptoid molecular transporters. *Proc. Natl. Acad. Sci. U.S.A.* **2000**, *97*, 13003–13008.

(15) Matsushita, M.; Tomizawa, K.; Moriwaki, A.; Li, S. T.; Terada, H.; Matsui, H. A high-efficiency protein transduction system demonstrating the role of PKA in long-lasting long-term potentiation. *J. Neurosci.* **2001**, *21*, 6000–6007.

(16) Takenobu, T.; Tomizawa, K.; Matsushita, M.; Li, S. T.; Moriwaki, A.; Lu, Y. F.; Matsui, H. Development of p53 protein transduction therapy using membrane-permeable peptides and the application to oral cancer cells. *Mol. Cancer Ther.* **2002**, *1*, 1043–1049.

(17) Wu, H. Y.; Tomizawa, K.; Matsushita, M.; Lu, Y. F.; Li, S. T.; Matsui, H. Poly-arginine-fused calpastatin peptide, a living cell membrane-permeable and specific inhibitor for calpain. *Neurosci. Res.* **2003**, *47*, 131–135.

(18) Rothbard, J. B.; Garlington, S.; Lin, Q.; Kirschberg, T.; Kreider, E.; McGrane, P. L.; Wender, P. A.; Khavari, P. A. Conjugation of arginine oligomers to cyclosporin A facilitates topical delivery and inhibition of inflammation. *Nature Med.* **2000**, *6*, 1253–1257.

(19) Marchand, C.; Zhang, X.; Pais, G. C. G.; Cowansage, K.; Neamati, N.; Burke, T. R., Jr.; Pommier, Y. Structural determinants for HIV-1 integrase inhibition by beta-diketo acids. *J. Biol. Chem.* **2002**, *277*, 12596–12603.

(20) Semenova, E. A.; Johnson, A. A.; Marchand, C.; Davis, D. A.; Tarchoan, R.; Pommier, Y. Preferential inhibition of the magnesium-dependent strand transfer reaction of HIV-1 integrase by alpha-hydroxytropolones. *Mol. Pharmacol.* **2006**, *69*, 1454–1460.

(21) Parniak, M. A.; Min, K. L.; Budihas, S. R.; Le Grice, S. F. J.; Beutler, J. A. A fluorescence-based high-throughput screening assay for inhibitors of HIV-1 reverse transcriptase associated ribonuclease H activity. *Anal. Biochem.* **2003**, *322*, 33–39.

(22) Morellet, N.; Bouaziz, S.; Petitjean, P.; Roques, B. P. NMR structure of the HIV-1 regulatory protein Vpr. *J. Mol. Biol.* **2003**, *327*, 215–227.

(23) Karki, R. G.; Tang, Y.; Burke, T. R., Jr.; Nicklaus, M. C. Model of full-length HIV-1 integrase complexed with viral DNA as template for anti-HIV drug design. *J. Comput.-Aided Mol. Des.* **2004**, *18*, 739–760.

(24) Wallace, A. C.; Laskowski, R. A.; Thormton, J. M. LIGPLOT—a program to generate schematic diagrams of protein ligand interactions. *Protein Eng.* **1995**, *8*, 127–134.

(25) Li, H.-Y.; Zawahir, Z.; Song, L.-D.; Long, Y.-Q.; Neamati, N. Sequence-based design and discovery of peptide inhibitors of HIV-1 integrase: insight into the binding mode of the enzyme. *J. Med. Chem.* **2006**, *49*, 4477–4486.

Gene Therapy (2010), 1–10

www.nature.com/gt

ORIGINAL ARTICLE

Improvement of lentiviral vector-mediated gene transduction by genetic engineering of the structural protein $Pr55^{Gag}$

T Aoki[1,2], S Shimizu[1], E Urano[1,3], Y Futahashi[1], M Hamatake[1], H Tamamura[2], K Terashima[4], T Murakami[1], N Yamamoto[1] and J Komano[1]

[1]*AIDS Research Center, National Institute of Infectious Diseases, Tokyo, Japan;* [2]*Department of Medicinal Chemistry, Institute of Biomaterials and Bioengineering, Tokyo Medical and Dental University, Tokyo, Japan;* [3]*Graduate School of Infection Control Sciences, Kitasato University, Tokyo, Japan and* [4]*Department of Comprehensive Pathology, Aging and Developmental Sciences, Tokyo Medical and Dental University, Graduate School, Tokyo, Japan*

The lentiviral vector is a promising tool for human gene therapy because of its ability to transduce genes into many cell types. However, one of the technical problems associated with the lentiviral vector is that lentiviral titers in current production systems are relatively low compared with the other viral vectors. In this study, we provide genetic evidence that the attachment of heterologous myristoylation (myr) signals on the amino-terminus of human immunodeficiency virus type 1 $Pr55^{Gag}$ (Gag) can increase the viral yield up to 10-fold, leading to the enhancement of gene transduction in many cell lines. The myr signal Gag constructs behaved similarly to the wild-type Gag in targeting to detergent-resistant membrane compartments, Vps4-dependence for viral budding, and virion morphology. However, the myr signal Gag constructs showed improved oligomerization efficiency as measured by bioluminescence resonance energy transfer in living cells, contributing to increased viral production and efficient activation of the viral protease responsible for virion maturation. The genetically modified Gag represents the next generation lentiviral vector, and should contribute to the success of many lentiviral vector applications.

Gene Therapy advance online publication, 22 April 2010; doi:10.1038/gt.2010.61

Keywords: *lentiviral vector; gag; myristoylation*

Introduction

The lentiviral vector is a powerful tool for transduction of genes into many cell types, especially non-dividing cells such as neurons, and is being used in clinical trials of human gene therapies and other applications.[1–8] The use of lentiviral vectors has been made possible because of advances in basic virology and because of a series of modifications that have increased the safety of the lentiviral vector. The commonly used third-generation lentiviral vector is a *Tat*-independent four-plasmid system composed of a gene transfer vector and three trans-vectors expressing Rev, Env and Gag-pol. The gene transfer vector is equipped with a self-inactivation LTR system (SIN). Viruses are often pseudotyped by vesicular stomatitis virus G (VSV-G). The human codon-optimized *gag-pol* expression vector is used to increase viral yield.[9]

The application of the lentiviral vector to human gene therapy was first approved for the treatment of human immunodeficiency virus (HIV) infections in the early 2000s.[1]. Since then, because of its potential advantages, the use of lentiviral vector has been expanding. A large amount of lentiviral particle must be produced for clinical trials. A technical improvement to increase the viral titer obtained from a production system would have a substantial effect on the cost of supporting a clinical human gene therapy trial using the lentiviral vector. The lentiviral vector titer in current production systems is generally in the order of 10^5–10^6 transducing units per ml. Although titer can be increased by centrifugation, the production yield is not as high as other viral vectors including the widely used adenoviral vectors. The HIV-1-based lentiviral vector has been engineered to reduce the risk of pathogenicity associated with HIV-1 [5,9], which resulted in a decrease of the viral titer.

Retroviral production and infectivity are regulated by the amino-terminal matrix domain ($p17^{MA}$ or MA) of $Pr55^{Gag}$ (Gag).[10–13] The myristoylation (myr) signal in the MA is critical for efficient viral production by aiding Gag trafficking to the plasma membrane (PM). In a previous study, we found that substitution of the HIV-1 Gag myr with the phospholipase C-δ1 pleckstrin homology (PH) domain increased the production of the third-generation lentiviral vector in which the *gag-pol* is human codon-optimized.[14] This prompted us to search for a PM-targeting signal that could enhance viral production to a greater extent than PH-Gag. Among the PM-targeting signals, we discovered that the myr signal motifs of

Correspondence: Dr J Komano, AIDS Research Center, National Institute of Infectious Diseases, 1-23-1 Toyama, Shinjuku, Tokyo, 162, Japan.
E-mail: ajkomano@nih.go.jp
Received 9 November 2009; revised 23 February 2010; accepted 7 March 2010

several heterologous proteins conferred such an effect. We suggest that the resulting modified Gag-based lentiviral vector can serve as a next generation lentiviral vector system, and should contribute to diverse applications of the lentiviral vector.

Results

We constructed HIV-1 Gag constructs (Figure 1a) containing the following PM-targeting proteins or PM-targeting signals fused to the Gag amino-terminus: the transmembrane proteins CD4, CD8, CXCR4, HIV-1 *Env*, or the acylation signal motifs of *lyn*, Gα(12), Gα(13) and Gα(16). This makes the original Gag myr signal unable to function. For CD4 and CXCR4, the full-length (FL) and cytoplasmic tail-deleted derivatives (DC) were examined. The membrane protein mutants are expected to traffic to the PM through the vesicular trafficking pathway involving ER and Golgi apparatus. As *lyn* encodes two overlapping acylation motifs, a myr and palmitoylation (pal) motif, we generated three *lyn*-derived constructs bearing a myr signal only, a pal signal only, or both signals (denoted myr^{lyn}, pal^{lyn}, myr/pal^{lyn}). In the *lyn* myr signal constructs, the position of the myristoyl group is –22 amino acids upstream from the original Gag context (denoted wild type, WT, hereafter). The *gag* and *env* sequences were human codon-optimized. The start codon and myr signal of Gag were destroyed by the M1L and G2A mutations to avoid internal translational initiation that could influence the experimental results.[14] The myr signal-defective Gag construct G2A was used as a negative control. PH-*gag* was used as a positive control that showed enhanced viral production.[14] The Gα(12), Gα(13) and Gα(16) constructs have one, two and three pal attachment sites, respectively. All the constructs were fused to green fluorescent protein (GFP), and expression was verified by western blot and immunoprecipitation analyses (Figure 1b).

A confocal microscopic analysis revealed that the majority of Gag-GFP was targeted to the PM, but some Gag-GFP was distributed in the cytoplasm with a fine vesicular pattern in 293FT cells (Figure 1c, WT). G2A-GFP showed a homogenous cytoplasmic distribution (Figure 1c). PH-Gag-GFP showed a distribution pattern similar to the WT (Figure 1c). These data are consistent with our previous findings.[14] The membrane protein Gag constructs mostly accumulated in the perinuclear region and only some of the protein was targeted to the PM, as verified by flow cytometric analysis using antibodies recognizing the extracellular domain of CD4, CD8 or CXCR4 (exemplified by the $CXCR4^{FL}$ mutant in Figure 1c, and data not shown). The myr/pal^{lyn} construct showed a phenotype similar to WT with fine vesicular staining close to the nucleus (Figure 1c). The myr^{lyn} construct showed a PM-targeting phenotype similar to WT (Figure 1c). The pal^{lyn} construct was distributed evenly in the cytoplasm similar to G2A (Figure 1c). The Gα constructs were distributed predominantly in the cytoplasm with vesicular staining patterns, and less evidently at the PM (exemplified by the Gα(16) construct in Figure 1c).

To evaluate the efficiency of virus-like particle (VLP) production, we measured the GFP fluorescence intensity of culture supernatants containing VLP relative to the cell fraction (Figure 1d). PH-*gag* showed a significant enhancement of VLP production (229.0%, Figure 1d) compared with Gag-GFP, and the G2A construct produced almost no VLP, consistent with previous findings.[14] Membrane protein mutants produced little VLP (0.8–41.6% relative to Gag-GFP), presumably because they were inefficiently transported to the PM as evidenced by the confocal microscopy analysis (Figure 1c). Among the membrane protein mutants, $CXCR4^{FL}$-*gag*-GFP showed the best VLP production efficiency (41.6% relative to Gag-GFP). Interestingly, deleting the cytoplasmic tail of CXCR4 led to a drastic loss of VLP production (0.8% relative to Gag-GFP), suggesting that the cytoplasmic tail of CXCR4 somehow contributes to VLP production. Myr/pal^{lyn}-*gag*-GFP showed significantly greater VLP production than the WT (229.4%, $P<0.05$, Student's *t*-test). Myr^{lyn}-*gag*-GFP produced slightly more VLP than the WT (131.5%). Pal^{lyn}-*gag*-GFP showed a weak VLP production ability (14.1%), possibly because the pal signal did not function effectively, or the palmitoyl group did not function as a PM-targeting motif in the given protein context. The Gα(12)- and Gα(13)-*gag*-GFP constructs, containing one or two pal motifs, respectively, showed 7.0 and 7.3% VLP production efficiencies, compared with the WT. The Gα(16)-*gag*-GFP construct, containing three pal motifs, was able to produce VLP (28.8%) more effectively than the other Gα constructs, suggesting that the pal group serves as a weak PM-targeting motif and that the motifs function additively. The two- to threefold enhancement of VLP production by PH- and myr/pal^{lyn}-gag-GFP was verified by western blot analysis examining the VLP fraction (data not shown). Overall, the GFP fluorescence-based VLP production assays were consistent with the microscopy observations indicating that the constructs that were able to target Gag to the PM were competent in VLP production (Figure 1c). These data indicate that the Gag constructs carrying *lyn* myr/pal or myr signals support VLP production more efficiently than the WT. Thus, we examined the infectivity of the lentiviral vectors produced by Gag with heterologous myr signals.

We constructed *gag-pol* derivatives bearing the myr/pal^{lyn} or myr^{lyn} sequences, and additional myr signal constructs carrying the myr signal of HIV-1 or MLV MA (myr^{HIV-1}- or myr^{MLV}-*gag-pol*, Figure 1a). These constructs were generated to examine whether any heterologous myr signal can function to enhance VLP production similar to the effect of the *lyn* acylation signal. In myr^{HIV-1}- or myr^{MLV}-*gag-pol*, the position of the myristoyl group is –22 amino acids upstream from the original Gag context, which is similar to the same position as myr/pal^{lyn} and myr^{lyn} mutants (Figure 1a). The expression of the *gag-pol* derivatives was verified by western blot analysis in which $Pr55^{Gag}$ and its cleaved products by viral protease including MA-CA and $p24^{CA}$ were detected (Figure 2a). These mutants produced VLP in the culture supernatant as verified by western blot analysis (Figure 2b). Using these *gag-pol* expression plasmids, in combination with the luciferase-encoding gene transfer plasmid and expression plasmids for Rev and VSV-G, we produced a lentiviral vector in 293FT cells. The viral production efficiencies were assessed by measuring the amount of viral capsid antigen $p24^{CA}$

a

Gag	MGARASVL...
G2A	MAARASVL...
PH-gag	(PLC delta 1 aa 1-175)-PRAE FTLAARASVL...
$CD4^{FL}$-gag	(CD4 aa 1-458)-E FTLAARASVL...
$CD4^{DC}$-gag	(CD4 aa 1-424)-E FTLAARASVL...
$CXCR4^{FL}$-gag	(CXCR4 aa 1-352)-EISSSSFE FTLAARASVL...
$CXCR4^{DC}$-gag	(CXCR4 aa 1-308)-ISSSSFE FTLAARASVL...
CD8-gag	(CD8 aa 1-235)-IDLELKL RILQSSSSFE FTLAARASVL...
Env-gag	(Env aa 1-869)-D PATGLRSRAE FTLAARASVL...
myr/pal^{lyn}-gag	MGCIKSKRKD NLNDDERRAE FTLAARASVL...
myr^{lyn}-gag	MGAIKSKRKD NLNDDERRAE FTLAARASVL...
pal^{lyn}-gag	MACIKSKRKD NLNDDERRAE FTLAARASVL...
Galpha(12)-gag	MS GVVRTLSRCL LPAEAGRRAE FTLAARASVL...
Galpha(13)-gag	MAD FLPSRSVCFP GCVLTNRRAE FTLAARASVL...
Galpha(16)-gag	MARSL RWRCCPWCLT EDEKAARRAE FTLAARASVL...
myr^{HIV-1}-gag	MGARASVLSG GELDRWRRAE FTLAARASVL...
myr^{MLV}-gag	MGQTVTTPLS LTLGHWRRAE FTLAARASVL...

b

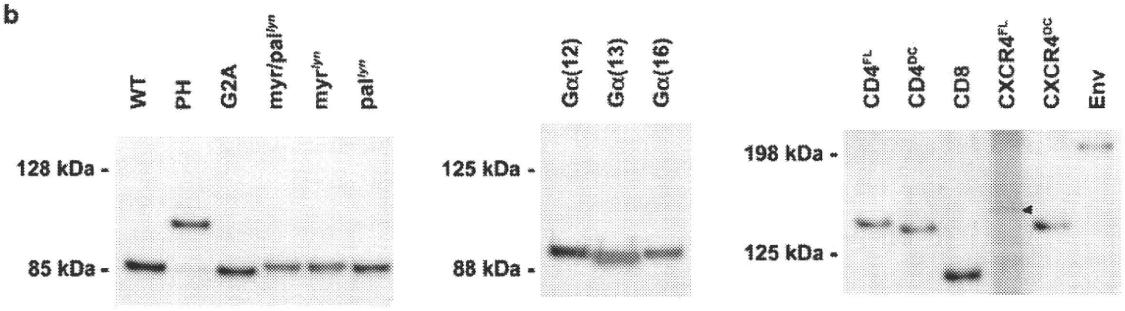

c

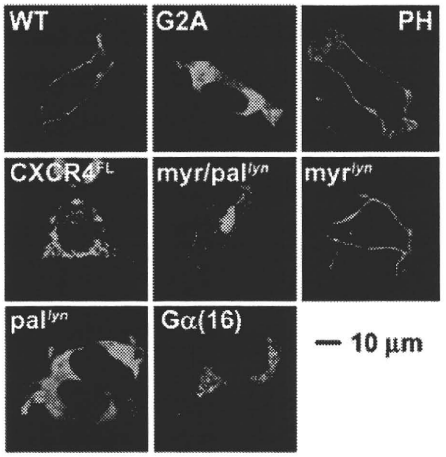

d VLP production efficiency (GFP fluorecence of VLP / cell fractions)

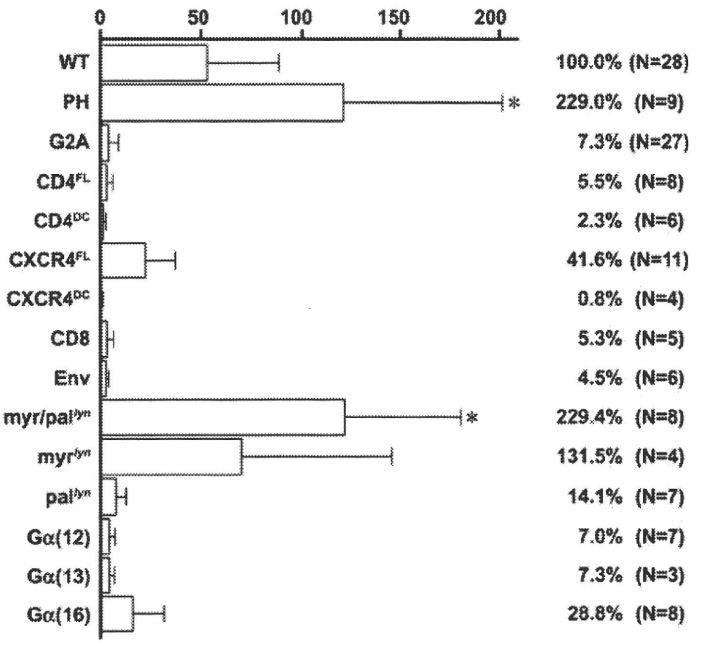

Figure 1 The production of VLPs by genetic modification of the PM-targeting signal of Gag. (**a**) The mutants used in this study. The myr site is marked with a dot, the palmitoylation site with an underline. The Gag translational initiation site and the myr target residues were mutated to leucine and alanine to minimize internal translational initiation and myr. (**b**) The verification of protein expression of Gag-GFP derivatives in 293FT cells by western blot analysis using anti-FLAG antibody. All the constructs carry the FLAG epitope at the C-terminus of Gag. The $CXCR4^{FL}$-Gag-GFP showed a low efficiency of detection, thus the immunoprecipitation was performed before immunoblotting (triangle). (**c**) The distribution of Gag-GFP derivatives in 293FT cells examined by confocal microscopy. WT represents the Gag-GFP, and the membrane-targeting signals are shown at the top of each panel. The bar represents 10 μm, magnification ×630. (**d**) VLP production efficiency of Gag-GFP derivatives measured by the GFP fluorescence in the VLP fraction divided by that of the cell fraction. The average and s.d. of the indicated number of independent experiments are shown. The VLP production efficiency relative to Gag-GFP is shown as a percentage at the right. Asterisks indicate the statistical significance compared with WT by two-tailed Student's *t*-test ($P<0.05$).

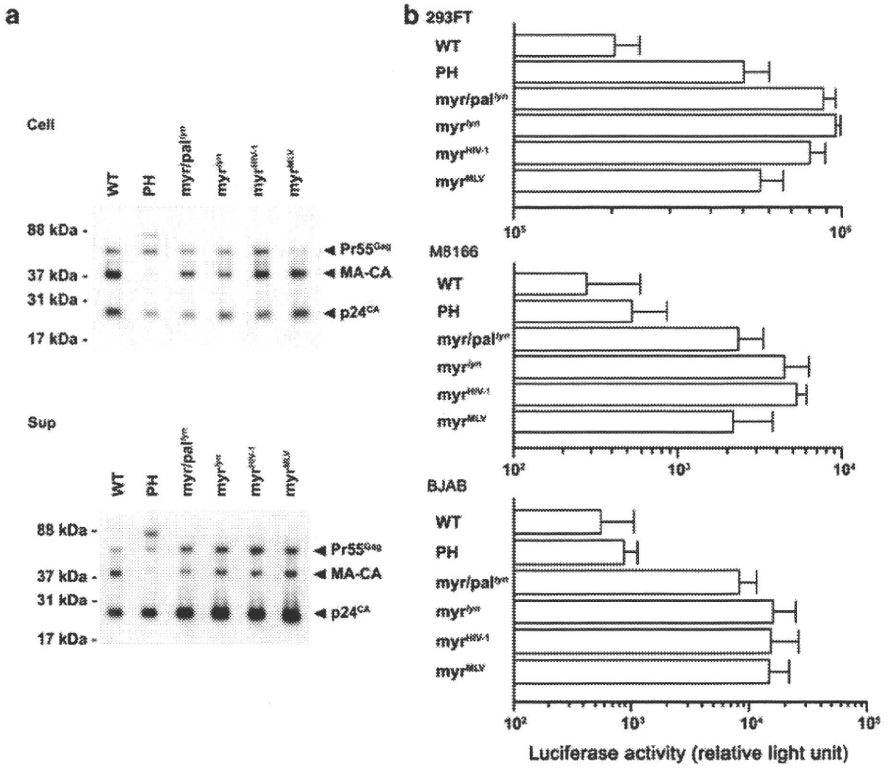

Figure 2 Lentiviral vector production and infectivity of myr signal mutants. (**a**) Verification of protein expression and VLP production of *gag-pol* derivatives in 293FT cells by western blot analysis using anti-p24^{CA} antibody. The upper panel shows the analysis of cell lysate equivalent to $1 \sim 2 \times 10^5$ cells (Cell). The lower panel shows the viral particles collected from the culture supernatant (Sup). Pr55^{Gag} (~55 kDa), the proteolytic cleavage intermediate of Pr55^{Gag} (MA-CA, ~40 kDa) and the complete proteolytic cleavage product p24^{CA} (~24 kDa) are indicated by arrowheads. PH-Gag has a higher molecular weight precursor and intermediate because of the PH domain of 23 kDa attached to the MA domain. (**b**) The transduction efficiency of the luciferase gene into various cell types. The 293FT, M8166 and BJAB cells were tested for luciferase gene transduction by the myr signal derivative lentivirus vectors. The *x* axis represents relative light emission. The average ± s.d. of luciferase activity assay in quadricate (293FT) or in triplicate (M8166 and BJAB) was shown. A representative data from three independent experiments is shown.

in the culture supernatant by enzyme-linked immunosorbent assay (ELISA). Enhancement of virus production by the PH, myr/pal^{lyn} and myr^{lyn} constructs was observed (4.1-, 6.3- and 10.5-fold increase in production, respectively, relative to the WT, Table 1). These data are consistent with the western blot analysis in which the levels of p24^{CA} are decreased from the cell fraction and increased in the VLP fraction for PH and myr signal mutants (Figure 2a). The magnitude of viral production enhancement was augmented in the *gag-pol* context compared with the Gag-GFP context. This is explained by the efficiency of Gag cleavage in the virion as described below. Viral production by the myr^{HIV-1}- or myr^{MLV}-*gag-pol* constructs also increased (6.2- or 6.1-fold, respectively, Table 1), suggesting that any heterologous myr signal can increase the production of lentiviral vector.

Luciferase gene transduction by lentiviral vectors produced using the modified Gag-pol was assessed in 293FT cells. The gene transduction efficiencies of *gag-pol* constructs were 6.1- to 10.9-fold greater than the WT (Figure 2b and Table 1). The luciferase activity decreased on treatment of the cells with the reverse transcriptase inhibitor nevirapine, suggesting that the luciferase activity indeed represents lentiviral gene transduction (data not shown). The increase in viral production by the heterologous myr signal constructs (4.3- to 7.8-fold compared with WT) largely agrees with the level of augmentation of luciferase activity (5.7- to 10.4-fold, Table 1). The myr/pal^{lyn} mutant showed a higher ratio (1.7) of luciferase transduction efficiency relative to viral production than the other myr signal mutants,

Table 1 Summary of viral production and infectivity of myr signal Gag mutants

	Viral production[a]	*Luciferase transduction*[b]	*Ratio*[c]
WT	1.0 ± 0.0 (n = 17)	1.0 ± 0.0 (n = 15)	1.0
PH	4.1 ± 0.9 (n = 17)**	6.3 ± 1.8 (n = 15)*	1.5
myr/pal^{lyn}	6.3 ± 1.8 (n = 17)*	10.4 ± 2.7 (n = 15)**	1.7
myr^{lyn}	10.5 ± 3.4 (n = 13)*	9.2 ± 3.2 (n = 11)*	0.9
myr^{HIV-1}	6.2 ± 1.9 (n = 12)*	5.7 ± 1.5 (n = 10)*	0.9
myr^{MLV}	6.1 ± 1.1 (n = 12)**	7.6 ± 2.7 (n = 10)*	1.2

Abbreviations: HIV-1, human immunodeficiency virus type 1; MLV, murine leukemia virus; myr, myristoylation; pal, palmitoylation; PH, pleckstrin homology; WT, wild type.
[a]The average ± s.e.m. of the p24^{CA} concentration relative to WT from the indicated number of independent experiments.
[b]The average ± s.e.m. of transduced luciferase activity relative to WT from the indicated number of independent experiments.
[c]The luciferase transduction divided by viral production.
Asterisks indicate a statistically significant difference compared to the WT by two-tailed Student's paired *t*-test (*$P < 0.05$, **$P < 0.01$).

suggesting that the infectivity of the myr/pal^{lyn} virus particles is slightly improved (Table 1). Luciferase gene transduction by myr signal constructs was also observed in the B lymphoid cell line BJAB and T lymphoid cell line M8166, similar to 293FT cells (Figure 2b). Gene transduction of GFP by myr signal *gag-pol* constructs was comparable to transduction of the luciferase gene (data not shown). Collectively, these results indicate that extending the amino-terminus of Gag with a heterologous myr signal enhances infectious lentiviral production.

We analyzed the molecular mechanisms by which viral production was improved by the amino-terminal Gag modifications. We examined (i) the oligomerization efficiency, (ii) the Vps4-dependence of viral budding, (iii) Gag targeting to the Triton X-100-insoluble lipid (detergent-resistant membrane, DRM) fraction and (iv) the morphology of the virion. First, the oligomerization efficiency was measured using a bioluminescent resonance energy transfer (BRET) assay (Figure 3a). The 293FT cells were co-transfected with plasmids expressing Gag derivatives fused to GFP or renilla luciferase (Rluc), and the GFP fluorescence activated by the Rluc-emitted light was measured in living cells. This BRET signal should represent the self-oligomerization efficiency of Gag derivatives *in vivo*. The GFP–Rluc fusion protein should yield the best BRET efficiency, and was thus used as the positive control. Rluc alone should not yield any BRET signal, and thus was used as a negative control. We focused on the derivatives that showed enhanced viral production. The BRET levels of all the tested mutants were significantly increased compared with the WT Gag (Figure 3a). These data imply that the assembly of the myr signal Gag constructs is more efficient than the WT. It is conceivable that the enhanced VLP production of myr signal Gag constructs is, in part, because of improved assembly efficiency. Efficient Gag assembly should also assist the Gag-pol assembly. The Gag-pol assembly leads to the activation of a viral protease that cleaves Gag to make the virus infectious. Provided that the myr signal Gag mutants can efficiently activate the viral protease, we expected that the Gag processing of myr signal Gag constructs should be more efficient than the WT. Virions were collected by centrifugation and processed for western blotting using the anti-p24^{CA} monoclonal antibody (mAb). Anti-p24^{CA} mAb binds to Pr55^{Gag} and its cleaved products including MA-CA and p24^{CA}. The p24^{CA} signal relative to the Pr55^{Gag} and MA-CA represents the Gag processing efficacy. Compared with cell lysates (Figure 2a), viral lysates showed better Gag cleavage for all samples (Figure 3b). The WT virions showed a substantial amount of Gag intermediates (Figure 3b). In contrast, only trace amounts of intermediate were detected in the myr signal construct virions (Figure 3b). It is possible that the enhanced Gag processing is due to the increased Gag-pol to Gag ratio in the virion produced by myr Gag mutants. We tested this possibility by western blot analysis probing p24^{CA} and integrase (IN) at the same time. IN represents the Gag-pol because IN is one of the proteolytic products generated from Gag-pol. The signal intensities of IN (open arrowhead, Figure 3b) relative to p24^{CA} (filled arrowhead, Figure 3b) for myr signal mutants were comparable to WT, suggesting that enhanced Gag processing is not due to the increased Gag-pol to Gag ratio in the virion

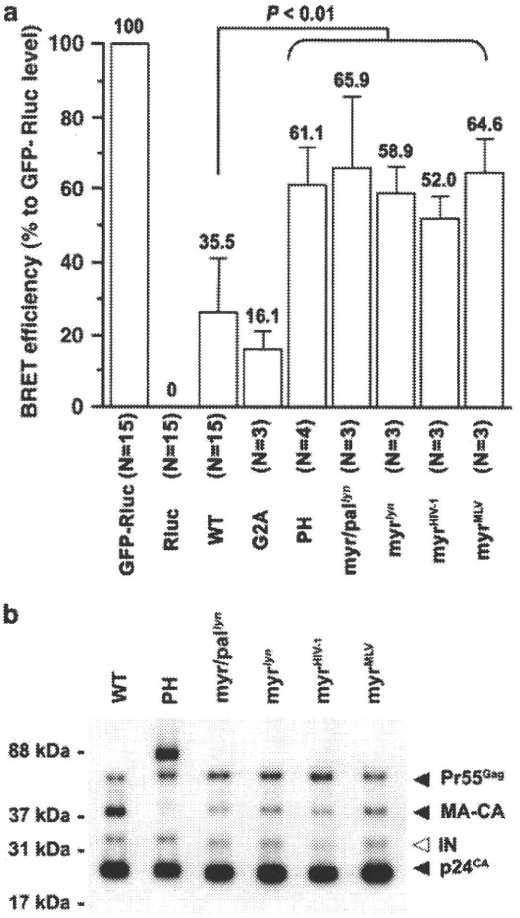

Figure 3 The physical and functional properties of myr signal derivatives of Gag. (**a**) Gag oligomerization examined by BRET analysis. The GFP–Rluc fusion protein and Rluc alone were used as positive and negative controls. The average ± s.d. of BRET efficiencies relative to the controls obtained in the indicated number of experiments are shown. All the *gag* mutants yielded significantly higher BRET signals than that of WT as analyzed by two-tailed Student's *t*-test ($P<0.01$). (**b**) The Gag processing and the Gag to Gag-pol ratio in the virion was tested by western blot analysis using anti-p24^{CA} and anti-IN monoclonal antibodies. Note that the samples were loaded to yield similar p24^{CA} signals to highlight the differences in Gag cleavage efficiencies and Gag to Gag-pol ratio. The virion was collected from the culture supernatant of cells shown in Figure 2a. Pr55^{Gag}, MA-CA, p24^{CA} (filled) and IN (open) are indicated by arrowheads.

produced by myr Gag constructs. Collectively, the results suggest that the heterologous myr signals enable Gag to assemble with a higher efficiency, leading to the activation of protease to process Gag more efficiently in the virion. This should account for the fact that the magnitude of difference between WT and mutants in VLP production was assessed greater by p24 ELISA assay using *gag-pol* constructs than by GFP fluorescence-based assay using Gag-GFP constructs.

Second, the Vps4-dependence of VLP budding was examined. Vps4 drives HIV-1 budding.[15] We measured VLP production efficiencies by *gag-pol* derivatives in the presence or absence of a dominant-negative Vps4. If VLP budding is powered by a Vsp4-independent mechanism, expression of dominant-negative Vps4 should not reduce the VLP production efficiency. Viral gene expression was

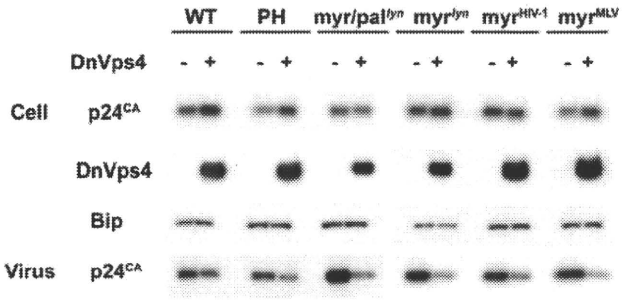

Figure 4 The effect of dominant-negative Vps4 (DnVps4) on virus production by acylation signal Gag derivatives. DnVps4 expression did not lower Gag expression in transiently transfected 293FT cells. In contrast, the virus production by all the Gag constructs was inhibited by DnVps4, similar to the WT.

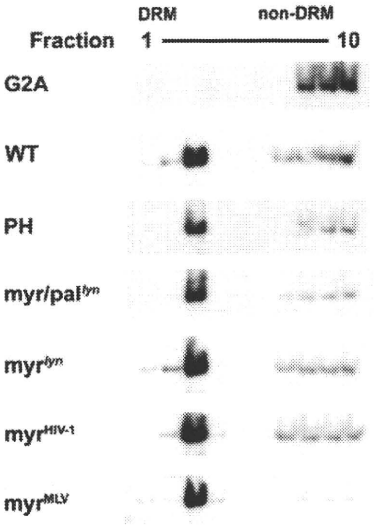

Figure 5 The targeting of Gag-GFP derivatives to the DRM fraction examined by a membrane floatation assay. G2A construct distributed to the non-DRM fractions (lanes 8–10), and WT Gag was targeted to the DRM (lanes 2–3). Other mutants distributed to the DRM fractions similar to WT Gag. All the derivatives were probed with anti-FLAG antibody.

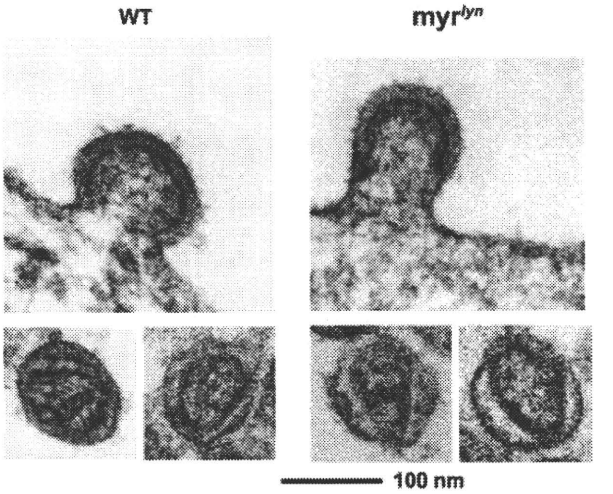

Figure 6 The morphology of virions produced from 293FT cells transiently transfected with *gag-pol* (WT, left) or myr^{lyn}-*gag-pol* (right) expression vector. The upper panels show viral budding at the cell periphery, and the lower panels show the morphology of virions found in the extracellular space. The bar represents 100 nm, magnification × 50 000.

not inhibited by dominant-negative Vps4 expression as judged by p24^{CA} levels (Figure 4). However, on expression of dominant-negative Vps4, viral production decreased in all the mutants (the lower panel of Figure 4), suggesting that the amino-terminal modification of Gag does not alter the molecular mechanism of viral budding.

Third, DRM targeting was examined using membrane floatation assays. Gag has previously been shown to form higher order complexes and bud at DRM-containing regions.[16,17] Increased viral production by myr signal Gag constructs may be due to improved efficiency of DRM targeting. In our experimental conditions, approximately 70% of Gag-GFP distributed to the DRM fractions (Figure 5). In contrast, G2A-GFP distributed predominantly to the non-DRM fractions (Figure 5). These data are consistent with the microscopy observations and previous reports (Figure 1c and Lindwasser and Resh[16] and Ono and Freed[17,18]). The myr signal derivatives accumulated in the DRM fractions at levels similar to the WT (Figure 5). These data suggest that enhanced viral production is not due to enhanced DRM targeting of Gag with amino-terminal modifications.

Finally, the morphology of the virion was analyzed using TEM. We compared the morphology of the WT and the myr^{lyn}-*gag-pol* virions. The morphology of budding and mature virions of myr^{lyn}-*gag-pol* construct was indistinguishable from the WT (Figure 6).[14] In addition, VSV-G was incorporated into the virion produced by myr signal derivatives at levels similar to the WT (data not shown). Similar observation was made for the incorporation of HIV-1 Env onto the virion (data not shown). The myr^{HIV-1}- and myr^{MLV}-Gag-GFP showed a PM-targeting phenotype similar to the WT as judged by confocal microscopy (data not shown). Taken together, lentiviral vectors bearing amino-terminally engineered Gag can produce virions with greater efficiencies than the original lentiviral vector. This increase was primarily attributed to the effects of the increased efficiency Gag oligomerization.

Discussion

In this study, we have provided evidence that genetic modification of the structural protein Gag can improve the virion production efficiency of the HIV-1-based lentiviral vector up to 10-fold. Our technology will provide an improved lentiviral vector for human gene therapy applications, which require large-scale viral vector preparation. Historically, efforts to improve the lentiviral vector have not involved the modification of the structural protein Gag.[9] Our strategy is unique in this regard. Our viral vector can be defined as a next generation lentiviral vector. This approach may also be worth testing for murine leukemia virus (MLV)-based vectors because the function of the MLV Gag is dependent on amino-terminal myr sites, similar to HIV Gag.

Our genetic approach revealed that amino-terminal modifications that re-position the myristoyl group attachment site on Gag can alter the late phases of the HIV-1 life cycle. Gag traffics to the PM efficiently, and the myristoyl group is critical for this process.[19] The myristoyl group attached to Gag is in equilibrium between exposed and folded 'hidden' conformations.[20] The PM targeting of Gag depends primarily on myristoyl group exposure. It is possible that re-positioning of the myristoyl group on Gag may slightly shift the structural equilibrium toward the exposed conformation, which facilitates PM targeting by Gag. However, myr signal Gag mutants did not show higher DRM-targeting efficiencies than WT (Figure 5). We performed the membrane floatation assay without Triton X-100 and found that the myr signal Gag mutants and WT distributed to the membrane fraction at similar efficiencies (data not shown). These data may suggest that the myristoyl group exposure model is unlikely. However, these data may not necessarily negate the myristoyl group exposure model because it is possible that the steady-state levels of Gag association with DRM could be saturable. Alternative hypothesis is that the re-positioning of myristoyl group may stabilize the Gag-PM association or Gag–Gag interaction, both of which should lead to an increased viral production.

Membrane proteins do not serve as an ideal PM-targeting motif for improvement of the lentiviral vector. The substitution of myr signal with membrane proteins appears to be less favorable because the PM-targeting efficiency of the membrane protein constructs was not high enough to produce VLP, probably because Gag starts to assemble on the ER membrane and bud into intracellular membrane compartments. This premature assembly may block the efficient ER exit of the membrane protein-Gag derivatives. In 293FT cells transiently transfected with plasmids expressing membrane Gag mutants, high electron density signals on the intracellular membranes and PM, representing assembled membrane protein-Gag mutants, were observed (data not shown). In addition, intracellular VLP formation was observed in intracellular membrane compartments surrounding the nucleus (data not shown). These observations were consistent with the confocal microscopy data, and suggest that the membrane protein-Gag constructs are assembly-competent. Interestingly, the morphology of the intracellular virion of CXCR4^{DC}-*gag-pol* was similar to late domain-defective HIV-1 particles. These data may imply that the membrane protein-Gag derivatives are not fully competent in VLP formation and/or release.

Considering our data, HIV-1 could have evolved to be able to produce more virus particles than it does now. However, such a virus was not selected in nature. This is presumably because the increased viral production may not confer a strong selective advantage for HIV-1 to spread in human population. It is possible that such a virus may kill the host, resulting in the loss of opportunity to be transmitted to a new host. Alternatively, such a virus may be more immunogenic, thus have selective disadvantage in the host. Conversely, it is possible that HIV-1 has already evolved to bud from its natural target cells, namely CD4-positive T lymphocytes or macrophages. If this is the case, our experimental observation might be only applied to the lentiviral vector production in 293FT cells.

Our next generation lentiviral vector should contribute to an increase in lentiviral vector applications, as a tool both for molecular biology research and for human gene therapy. The safety concerns involving Gag amino-terminal modification should be critically examined to use the modified lentiviral vector in clinical trials because the effect of amino-terminal modification of Gag on the lentiviral life cycle is unpredictable. The amino-terminal modification of Gag may alter the chromosomal integration site preference of the lentiviral vector genome. A genome-wide survey to determine the cellular genomic loci in which the Gag-modified lentiviral vector preferentially inserts its genome, compared with the original viral vector, should be conducted. In addition, it may be important to measure the frequency of insertional oncogenesis using small animal models. It is also possible that the fidelity of reverse transcription could be affected by the Gag amino-terminal modification. If the accuracy of reverse transcription drops, the therapeutic effect of the modified lentiviral vector might be affected. These issues should be addressed before the modified lentiviral vector is applied to human gene therapy.

We may be able to further improve the lentiviral vector using systematic modifications of Gag, but such an approach has yet to be examined. For example, the positioning the myr attachment site in all the myr signal Gag derivatives tested in this study was –22 amino acids relative to the original position. A better myristol group-positioning site or other PM-targeting signals to boost viral production and infectivity could be identified by performing an exhaustive systematic modification study.

Materials and methods

Plasmids

The codon optimized HIV-1 *gag* was amplified by PCR from pSyn HIV-1 *gag-pol*[21] using the following primers: HIV-1 *gag* forward 5′-ACCGGTCTCGAGCCACCAT GGGCGCCAGGGCCAGCGTGCTGAGC-3′, HIV-1 *gag* reverse 5′-TCATTGGATCCGGTCGTCATCGTCTTTGT AGTCTTGTGACGAGGGGTCGTTGCCAAAG-3′. The PCR fragment was cloned into pCR4 Blunt TOPO (Invitrogen, Tokyo, Japan), digested with *Xho*I–*Bam*HI, and the resulting fragment was cloned into the *Xho*I–*Bam*HI sites of pEGFP-N2 (Clontech, Palo Alto, CA, USA), generating pGag-GFP. A FLAG epitope tag was encoded at the carboxy-terminus of Gag. The LA-*gag* has been described previously.[14] The *Sna*BI–*Sac*II fragment from pLA-*gag-pol* was cloned into the *Sna*BI–*Sac*I sites of pSyn HIV-1 *gag-pol*, generating the pLA-*gag*-GFP.

The CD4 FL or DC was amplified from CD4 complementary DNA[22] using the following primers: FL and DC forward 5′-GGATCCCGGGCCACCATGAACCG GGGAGTCCCTTTTAGGC-3′, FL reverse 5′-GAATT CAATGGGGCTACATGTCTTCTGAAACCGG-3′, and DC reverse 5′-GAATTCGTGCCGGCACCTGACACAGAAG AAGATGCC-3′. The PCR fragments were cloned into pCR4 Blunt TOPO (Invitrogen), digested with *Bam*HI–*Eco*RI, and the resulting fragments were cloned into the *Bgl*II*Eco*RI sites of pEGFP-N2, generating pCD4$^{FL/DC}$-GFP. The *Sna*BI–*Eco*RI fragments from pCD4$^{FL/DC}$-GFP were cloned into the corresponding sites of pLA-*gag*-GFP, generating pCD4$^{FL/DC}$-*gag*-GFP.

The full-length human CD8 ORF was amplified by reverse transcriptase-PCR using mRNA isolated from peripheral blood mononuclear cell (PBMC) with following primers: 5′-GCTAGCATGGCCTTACCAGTGAC-3′and 5′-AGATCTATGACGTATCTCGCCGAAAGGCT-G-3′. An *Nhe*I–*Bgl*II fragment was cloned into the corresponding sites of pEGFP-N1 (Clontech), generating pEGFPN1hCD8. The *Sna*BI–*Sal*I fragment from pEGFPN1hCD8 was cloned into the *Sna*BI–*Xho*I site of pCXCR4^{FL}-*gag*-GFP, generating pCD8-*gag*-GFP.

The CXCR4 FL and DC were amplified from the CXCR4 complementary DNA[22] using the following primers: FL and DC forward 5′-ACCGGTGCCACCATG GAGGGGATCAGTATATACACTTCAG-3′, FL reverse 5′-AGATCTCGCTGGAGTGAAAACTTGAAGACTCAGA CTC-3′, and DC reverse 5′-AGATCTTGGCTCCAAG GAAAGCATAGAGGATGGG-3′. The *Age*I–*Bgl*II fragments of the PCR products were cloned into *Age*I–*Bgl*II sites of pEGFP-C2, generating pCXCR4$^{FL/DC}$-GFP. The *Sna*BI–*Eco*RI fragments from pCXCR4$^{FL/DC}$-GFP were cloned into the corresponding sites of pLA-*gag*-GFP, generating pCXCR4$^{FL/DC}$-*gag*-GFP.

The following oligonucleotides were annealed and cloned into the BsrGI site of pEGFP-N2 to generate pEGFP-N2-FLAG: 5′-GTACGACTACAAAGACGATGA CGACTATAAGTAAGC-3′ and 5′-GGCCGCTTACTTA TAGTCGTCATCGTCTTTGTAGTC-3′. HIV-1 Env was amplified from pgp160opt that encodes a codon-optimized gp160 (obtained through the NIH AIDS Research and Reference Reagent Program[23]) using the following primers: 5′-GGAACTGGTTCGACATCACCAAGTGGCT GTGG-3′ and 5′-GTTAACCCCGGGATCCAGCAGGGC GGTCTCGAAGCCCTGGCGGATGCGGC-3′. The *Bgl*II–*Xma*I fragment of the PCR product was cloned into pEGFP-N2 flag, generating pgp160opt3fwd2revEGFPN2f. The *Nde*I–*Sfi*I fragment from pgp160opt was cloned into pgp160opt3fwd2revEGFPN2f, generating pgp160optGFPf. The *Afe*I–*Mfe*I fragment carrying *gag*-GFP was cloned into the pgp160optGFPf, generating pEnv-*gag*-GFP.

The PH domain of phospholipase C-δ1 from pGFP-PH (generous gift from Dr Meyer's group,[24]) was amplified using following primers: forward 5′- CGCTAGCACC GGTGCCACCATGGACTCGGGCCGGGACTTCCTG-3′ and reverse 5′- CCTCGAGGCTGGATGTTGAGCTCCTT CAGG-3′. The *Nhe*I–*Xho*I fragment of the PCR product was cloned into the corresponding sites of pLA-*gag*-GFP, generating pPH-*gag*-GFP.

The following oligonucleotides were annealed and inserted into the *Nhe*I–*Xho*I sites of pLA-*gag*-GFP to generate pmyr/pal^{lyn}-*gag*-GFP, pmyr^{lyn}-*gag*-GFP, ppal^{lyn}-*gag*-GFP, pGα (12)-*gag*-GFP, pGα (13)-*gag*-GFP, pGα (16)-*gag*-GFP, pmyr^{MLV}-*gag*-GFP, pmyr^{HIV-1}-*gag*-GFP: myr/pal^{lyn} forward 5′- CTAGCGCCACCATGGGCTGCAT CAAGTCCAAGCGGAAGGACAACTTGAACGACGAC GAGCG-3′ and myr/pal^{lyn} reverse 5′- TCGACGCTC GTCGTCGTTCAAGTTGTCCTTCCGCTTGGACTTGAT GCAGCCCATGGTGGCG-3′; myr^{lyn} forward 5′- CTAGC GCCACCATGGGCGCCATCAAGTCCAAGCGGAAGG ACAACTTGAACGACGACGAGCG-3′ and myr^{lyn} reverse 5′- TCGACGCTCGTCGTCGTTCAAGTTGTCCT TCCGCTTGGACTTGATGGCGCCCATGGTGGCG-3′; pal^{lyn} forward 5′- CTAGCGCCACCATGGCATGTATTAA ATCAAAAAGGAAAGACCg-3′ and pal^{lyn} reverse 5′- TC GACGGTCTTTCCTTTTTGATTTAATACATGCCATGGT GGCG-3′; Gα(12) forward 5′- CTAGCGCCACCATGT CCGGCGTGGTGCGGACCCTGTCCCGGTGCCTGCTG CCCGCCGAAGCCGGCCG-3′ and Gα(12) reverse 5′- TC GACGGCCGGCTTCGGCGGGCAGCAGGCACCGGGA CAGGGTCCGCACCACGCCGGACATGGTGGCG-3′; Gα(13) forward 5′- CTAGCGCCACCATGGCCGACTTC CTGCCCTCCCGGTCCGTGTGCTTCCCCGGCTGCGTG CTGACCAACCG-3′ and Gα(13) reverse 5′- TCGACGG TTGGTCAGCACGCAGCCGGGGAAGCACACGGACCG GGAGGGCAGGAAGTCGGCCATGGTGGCG-3′; Gα(16) forward 5′- CTAGCGCCACCATGGCCCGGTCCCTGCG GTGGCGGTGCTGCCCCTGGTGCCTGACCGAGGACGA GAAGGCCGCCCG-3′ and Gα(16) reverse 5′- TCGAC GGGCGGCCTTCTCGTCCTCGGTCAGGCACCAGGGGC AGCACCGCCACCGCAGGGACCGGGCCATGGTGGC G-3′; myr^{HIV-1} forward 5′- CTAGCGCCACCATGGGCG CCAGGGCCAGCGTGCTGAGCGGCGGCGAGCTGGAC AGGTGGCG-3′ and myr^{HIV-1} reverse 5′- TCGACGC CACCTGTCCAGCTCGCCGCCGCTCAGCACGCTGGCC CTGGCGCCCATGGTGGCG-3′; myr^{MLV} forward 5′- CTA GCGCCACCATGGGCCAGACTGTTACCACTCCCTTAAG TTTGACCTTAGGTCACTGGCG-3′ and myr^{MLV} reverse 5′- TCGACGCCAGTGACCTAAGGTCAAACTTAAGGGA GTGGTAACAGTCTGGCCCATGGTGGCG-3′. The *Sna*BI–*Sac*II fragments from pmyr/pal^{lyn}-*gag*-GFP, pmyr^{lyn}-*gag*-GFP, pmyr^{MLV}-*gag*-GFP and pmyr^{HIV-1}-*gag*-GFP were cloned into the corresponding sites of pSyn HIV-1 *gag-pol* to generate pmyr/pal^{lyn}-*gag-pol*, pmyr^{lyn}-*gag-pol*, pmyr^{MLV}-*gag-pol* and pmyr^{HIV-1}-*gag-pol*, respectively.

The following linkers were inserted into the *Bam*HI site of the pGag-GFP, to generate the pHIV-1 *gag*f AB linker: 5′-GATCAAGGATCCACCGGTAGATCTGACCG GTGGATCCTT-3′ and 5′-GATCAAGGATCCACCGGT CAGATCTACCGGTGGATCCTT-3′. The firefly luciferase open reading frame was amplified by PCR using the following primers: 5′-ACCGGTCTCGAGGGCCAC CATGGAAGACGCCAAAAACATAAAGAAAGG-3′ and 5′-GAATTCGGATCCTTACACGGCGATCTTTCCGCCCT TCTTGGCC-3′. The *Age*I–*Eco*RI fragment of the PCR product was cloned into the *Bam*HI site of the pHIV-1 *gag*f AB linker, producing pGag-fLuc. The *Nhe*I–*Xba*I fragment from phRL-CMV (Promega, Tokyo, Japan) was inserted into the *Bam*HI site of pGag-fLuc, generating the pGag-Rluc II, using the following linkers: *Nhe*I side, 5′-GATCTGGTTACCCAATTG-3′ and 5′-CTAGCAATTG GGTAACCA-3′; *Xba*I side, 5′-CTAGCGAATTCA-3′ and 5′-GATCTGAATTCG-3′.

The *Nde*I–*Sac*II fragment from pPH-*gag*-GFP[14] was cloned into the corresponding sites of pGag-Rluc II, generating pPH-*gag*-Rluc. The *Apa*I–*Hpa*I fragments from pmyr/pal^{lyn}-*gag*-GFP, pmyr^{lyn}-*gag*-GFP, pmyr^{MLV}-*gag*-GFP and pmyr^{HIV-1}-*gag*-GFP were cloned into the corresponding sites of pGag-Rluc II, generating pmyr/pal^{lyn}-*gag*-Rluc, pmyr^{lyn}-*gag*-Rluc, pmyr^{MLV}-*gag*-Rluc and pmyr^{HIV-1}-*gag*-Rluc, respectively.

The Vps4DN expression vector was the generous gift of Dr H Gottlinger (University of Massachusetts). Other plasmids including pLenti-luciferase, pVSV-G and pRevpac have been described previously.[14]

Cells and transfection

Cells were maintained in RPMI 1640 medium (Sigma, St Louis, MA, USA) supplemented with 10% fetal bovine serum (Japan Bioserum, Tokyo, Japan), 50 U ml^{-1} penicillin and 50 μg ml^{-1} streptomycin (Invitrogen), at 37 °C in a humidified 5% CO_2 atmosphere. Cells were

transfected with Lipofectamine 2000 according to the manufacturer's protocol (Invitrogen).

Western blotting

Transfected 293FT cells were washed once with Dullbeco's phosphate-buffered saline (Sigma), centrifuged and lysed in a buffer containing 0.31 M Tris-HCl (pH 6.8), 10% (w/v) sodium dodecyl sulfate, 50% (v/v) glycerol, 500 mM dithiothreitol and 0.25% (w/v) bromophenol blue. Proteins were separated by sodium dodecyl sulfate–polyacrylamide gel electrophoresis and transferred to polyvinylidine difluoride membranes (Millipore, Tokyo, Japan). Membranes were incubated with primary antibodies including polyclonal anti-flag (Rockland Immunochemicals, Gilbertsville, PA, USA), anti-$p24^{CA}$ mAb clone 183-H12-5C (NIH AIDS Research and Reference Reagent Program), anti-HIV-1 IN mAb clone ab72007 (Abcam, Cambridge, MA, USA) or anti-Bip mAb clone 40 (BD Biosciences, Tokyo, Japan), followed by a horseradish peroxidase conjugated secondary antibody (Envision, Dako, Tokyo, Japan). Chemiluminescence was generated using Lumilight (Roche, Tokyo, Japan) or Lumigen (GE Healthcare, Tokyo, Japan). Signals were detected using an LAS-3000 mini Lumino-Image analyzer operated by the LAS-300 mini Image Reader software (ver.2.2, Fuji Film, Tokyo, Japan). The brightness and contrast of the image were adjusted using Adobe Photoshop (ver.7.0, Adobe, Tokyo, Japan).

Confocal microscopy

Transfected 293FT cells were grown on slide glass in the presence of Hoechst 33258 (Sigma) for 24 h, fixed (4% formaldehyde), mounted and analyzed using confocal fluorescence microscopy (LSM510 Meta 63 × NA 1.4 lens, Carl Zeiss MicroImaging Inc., Tokyo, Japan). The brightness and contrast of the image were adjusted using the LSM image browser (Carl Zeiss).

VLP assay

Transfected 293FT cells were washed once with phosphate-buffered saline, centrifuged and lysed in buffer A (150 mM NaCl, 50 mM Tris-HCL (pH 8.0), 0.5% IGEPAL CA-630) for 0.5–1 h on ice (cell fraction). The cell culture medium was collected, passed through a 0.45 μm filter, and VLP were pelleted by ultracentrifugation (541 k × *g* for 1 h). The VLP pellet was lysed in buffer A for 0.5–1 h (VLP fraction). The green fluorescent intensities of cell and VLP fractions were quantified with a DTX880 Multimode Detector (excitation 485 nm, emission 535 nm) (Beckman Coulter, Tokyo, Japan). The efficiency of VLP production was calculated by dividing the green fluorescent intensity of the VLP fraction by that of the cell fraction.

Infection with lentiviral vector

The 293FT cells grown in six-well plates were transfected with *gag-pol* vector (1 μg), pLenti-luciferase (0.65 μg), pVSV-G (0.4-0.8 μg) or pRevpac (0.05 μg) using Lipoftamine 2000, and replated into three wells of a six-well plate at 4–6 h after transfection. At 48 h after transfection, the cell culture medium was collected, passed through a 0.45 μm filter (Millex-HV polyvinylidine difluoride; Millipore), and mixed with dextran (final concentration 16.25 μg ml^{-1}; DEAE-Dextran chloride, MW ~500 kDa; ICN Biomedicals Inc., Aurora, OH, USA). The 293FT cells at 50% confluency in 24-well plates were exposed to 800 μl of cell culture medium containing viruses. At 4–6 h after infection, 293FT cells were split into 4 wells of a 48-well plate. At 48 h after infection, the luciferase activity was measured using the Steady-Glo Luciferase Assay system (Promega). Luminescence was detected using a Veritas Microplate Luminometer (Promega).

Enzyme-linked immunosorbent assay

A p24 ELISA was conducted according to the manufacturer's protocol (Zeptometrics, Buffalo, NY, USA). To measure cellular p24, transfected 293FT cells were washed once with phosphate-buffered saline, lysed in 500 μl buffer A (described above) for 30 min, and subjected
to the ELISA.

Bioluminescence resonance energy transfer

The basic protocol for the BRET assay has been described previously.[25] Briefly, 293FT cells grown in a six-well plate were transfected with 0.05–0.2 μg of expression plasmids for Gag derivatives fused to the Rluc together with 1–2 μg of Gag derivatives fused to GFP. At 48 h after transfection, cells were collected and incubated with the Rluc substrate according to the manufacturer's protocol, with the exception that a 5- to 10-fold higher substrate concentration was used (ViviRen Live Cell Substrate; Promega). We measured BRET signals under the conditions in which the GFP and Rluc expression levels were almost similar among the tested samples. The fluorescent and bioluminescent signals were measured using a Tristar LB941 instrument (Berthold Technologies, Bad Wildbad, Germany).

Membrane floatation assay

293FT cells were transfected with a *gag* expression vector using Lipofectamine 2000 (Invitrogen) according to the manufacturer's protocol. At 48 h after transfection, cells were rinsed with ice-cold phosphate-buffered saline and centrifuged at 600 × *g* for 5 min. Cell pellets were resuspended in a buffer containing 10 mM Tris-Cl (pH 7.5), 4 mM EDTA and protease inhibitor cocktail (Sigma), and sonicated on ice. Cell lysates were centrifuged at 370 × *g* for 3 min. A 120 μl aliquot of supernatant was mixed with 3.6 μl 5 M NaCl (final concentration = 150 mM) and 120 μl of TNE-T (100 mM Tris-Cl (pH 7.5), 600 mM NaCl, 16 mM EDTA and 0.5% Triton X-100). These samples were placed on ice for 20 min. Subsequently, 200 μl of supernatant was mixed with 1 ml of 85.5% (wt/vol) sucrose in TNE and placed on the bottom of a centrifuge tube (Ultra Clear, Beckman Coulter), overlayed with 2.8 ml 65% and 1.2 ml 10% (wt/vol) sucrose in TNE-T without Triton X-100 (TNE), respectively. The gradient solution was centrifuged for 16 h at 1 48 862 × *g* at 4 °C in a BECKMAN SW55Ti rotor and 10 fractions of 500 μl each were recovered from top-to-bottom.

Transmission electron microscopy (TEM)

Transmission electron microscopy imaging was conducted by Hanaichi Co Ltd (Okazaki, Japan). Transfected 293FT cells were removed culture medium, fixed (2% glutaraldehyde, 2% osmium tetroxide), and imaged by transmission electron microscopy (at 100 kV;

JEOL JEM2000EX, Japan Electron Optics Laboratory Co., Ltd., Tokyo, Japan).

Conflict of interest

The authors declare no conflict of interest.

Acknowledgements

This work was supported by the Japan Health Science Foundation, the Japanese Ministry of Health, Labor and Welfare (H18-AIDS-W-003 to JK) and the Japanese Ministry of Education, Culture, Sports, Science and Technology (18689014 and 18659136 to JK).

References

1 MacGregor RR. Clinical protocol. A phase 1 open-label clinical trial of the safety and tolerability of single escalating doses of autologous CD4T cells transduced with VRX496 in HIV-positive subjects. *Hum Gene Ther* 2001; **12**: 2028–2029.
2 Hofling AA, Devine S, Vogler C, Sands MS. Human CD34+ hematopoietic progenitor cell-directed lentiviral-mediated gene therapy in a xenotransplantation model of lysosomal storage disease. *Mol Ther* 2004; **9**: 856–865.
3 Bank A, Dorazio R, Leboulch P. A phase I/II clinical trial of beta-globin gene therapy for beta-thalassemia. *Ann NY Acad Sci* 2005; **1054**: 308–316.
4 Manilla P, Rebello T, Afable C, Lu X, Slepushkin V, Humeau LM *et al.* Regulatory considerations for novel gene therapy products: a review of the process leading to the first clinical lentiviral vector. *Hum Gene Ther* 2005; **16**: 17–25.
5 Cockrell AS, Kafri T. Gene delivery by lentivirus vectors. *Mol Biotechnol* 2007; **36**: 184–204.
6 Lundberg C, Björklund T, Carlsson T, Jakobsson J, Hantraye P, Déglon N *et al.* Applications of lentiviral vectors for biology and gene therapy of neurological disorders. *Curr Gene Ther* 2008; **8**: 461–473.
7 Maetzig T, Galla M, Brugman MH, Loew R, Baum C, Schambach A. Mechanisms controlling titer and expression of bidirectional lentiviral and gammaretroviral vectors. *Gene Ther* 2010; **17**: 400 .
8 ter Brake O, Berkhout B. Lentiviral vectors that carry anti-HIV shRNAs: problems and solutions. *J Gene Med* 2007; **9**: 743–750.
9 McCart JA, Bartlett DI. Lentiviral vectors. In: Templeton NS (ed). *Gene and Cell Therapy: Therapeutic Mechanisms and Strategies*, rd edn CRC Press: Carrollton, 2008, pp 245–262.
10 Fiorentini S, Marini E, Caracciolo S, Caruso A. Functions of the HIV-1 matrix protein p17. *New Microbiol* 2006; **29**: 1–10.
11 Hearps AC, Jans DA. Regulating the functions of the HIV-1 matrix protein. *AIDS Res Hum Retroviruses* 2007; **23**: 341–346.
12 Bukrinskaya A. HIV-1 matrix protein: a mysterious regulator of the viral life cycle. *Virus Res* 2007; **124**: 1 .
13 Klein KC, Reed JC, Lingappa JR. Intracellular destinies: degradation, targeting, assembly, and endocytosis of HIV Gag. *AIDS Rev* 2007; **9**: 150–161.
14 Urano E, Aoki T, Futahashi Y, Murakami T, Morikawa Y, Yamamoto N *et al.* Substitution of the myristoylation signal of human immunodeficiency virus type 1 Pr55Gag with the phospholipase C-delta1 pleckstrin homology domain results in infectious pseudovirion production. *J Gen Virol* 2008; **89**: 3144–3149.
15 Garrus JE, von Schwedler UK, Pornillos OW, Morham SG, Zavitz KH, Wang HE *et al.* Tsg101 and the vacuolar protein sorting pathway are essential for HIV-1 budding. *Cell* 2001; **107**: 55–65.
16 Lindwasser OW, Resh MD. Multimerization of human immunodeficiency virus type 1 Gag promotes its localization to barges, raft-like membrane microdomains. *J Virol* 2001; **75**: 7913–7924.
17 Ono A, Freed EO. Plasma membrane rafts play a critical role in HIV-1 assembly and release. *Proc Natl Acad Sci USA* 2001; **98**: 13925–13930.
18 Ono A, Freed EO. Binding of human immunodeficiency virus type 1 Gag to membrane: role of the matrix amino terminus. *J Virol* 1999; **73**: 4136–4144.
19 Gottlinger HG, Sodroski JG, Haseltine WA. Role of capsid precursor processing and myristoylation in morphogenesis and infectivity of human immunodeficiency virus type 1. *Proc Natl Acad Sci USA* 1989; **86**: 5781–5785.
20 Zhou W, Resh MD. Differential membrane binding of the human immunodeficiency virus type 1 matrix protein. *J Virol* 1996; **70**: 8540–8548.
21 Wagner R, Graf M, Bieler K, Wolf H, Grunwald T, Foley P *et al.* Rev-independent expression of synthetic gag-pol genes of human immunodeficiency virus type 1 and simian immunodeficiency virus: implications for the safety of lentiviral vectors. *Hum Gene Ther* 2000; **11**: 2403–2413.
22 Komano J, Miyauchi K, Matsuda Z, Yamamoto N. Inhibiting the Arp2/3 complex limits infection of both intracellular mature vaccinia virus and primate lentiviruses. *Mol Biol Cell* 2004; **15**: 5197–5207.
23 Gao F, Li Y, Decker JM, Peyerl FW, Bibollet-Ruche F, Rodenburg CM *et al.* Codon usage optimization of HIV type 1 subtype C gag, pol, env, and nef genes: *in vitro* expression and immune responses in DNA-vaccinated mice. *AIDS Res Hum Retroviruses* 2003; **19**: 817–823.
24 Stauffer TP, Ahn S, Meyer T. Receptor-induced transient reduction in plasma membrane PtdIns(4,5)P2 concentration monitored in living cells. *Curr Biol* 1998; **8**: 343–346.
25 Hamatake M, Aoki T, Futahashi Y, Urano E, Yamamoto N, Komano J. Ligand-independent higher-order multimerization of CXCR4, a G-protein-coupled chemokine receptor involved in targeted metastasis. *Cancer Sci* 2009; **100**: 95 .

 DOI 10.1002/eji.200939479 Eur. J. Immunol. 2010. 40: 1504–1509

European Journal of Immunology

SHORT COMMUNICATION

Inhibition of HIV replication by a CD4-reactive Fab of an IgM clone isolated from a healthy HIV-seronegative individual

Makiko Hamatake[1], Jun Komano[1], Emiko Urano[1], Fumiko Maeda[2], Yasuko Nagatsuka[3] and Masataka Takekoshi[2]

[1] AIDS Research Center, National Institute of Infectious Diseases, Tokyo, Japan
[2] Department of Molecular Life Science, Division of Basic Molecular Science and Molecular Medicine, Tokai University School of Medicine, Isehara, Japan
[3] Laboratory for Molecular Membrane Neuroscience, Brain Science Institute, RIKEN, Wako, Saitama, Japan

HIV replication is restricted by some anti-CD4 mouse mAb *in vitro* and *in vivo*. However, a human monoclonal anti-CD4 Ab has not been isolated. We screened EBV-transformed peripheral B cells from 12 adult donors for CD4-reactive Ab production followed by functional reconstitution of Fab genes. Three independent IgM Fab clones reactive specifically to CD4 were isolated from a healthy HIV-seronegative adult (~0.0013% of the peripheral B cells). The germ line combinations for the V_H and V_L genes were V_H3-33/$_L$6, V_H3-33/$_L$12, and V_H4-4/$_L$12, respectively, accompanied by somatic hypermutations. Genetic analysis revealed a preference for V-gene usage to develop CD4-reactive Ab. Notably, one of the CD4-reactive clones, HO538-213, with an 1×10^{-8}M dissociation constant (Kd) to recombinant human CD4, limited the replication of R5-tropic and X4-tropic HIV-1 strains at 1–2.5 μg/mL in primary mononuclear cells. This is the first clonal genetic analysis of human monoclonal CD4-reactive Ab. A mAb against CD4 isolated from a healthy individual could be useful in the intervention of HIV/AIDS.

Key words: Autoimmunity · CD4-reactive Ab · IgM · Inhibition of HIV replication

Supporting Information available online

Introduction

CD4 is a T-cell marker that serves as a principal receptor for HIV. CD4-reactive Ab are detected in HIV-infected individuals (~13%) [1, 2] and HIV-exposed seronegative individuals (34%) [3]. In addition, some healthy individuals are positive for anti-CD4 Ab (~0.6%) [4]. Replication of multiple HIV clades is blocked by mouse mAb against CD4 *in vitro* and *in vivo* [5–12]. Thus, it is possible that anti-CD4 Ab play a role in protecting individuals from HIV infection and delaying AIDS disease progression. Similar arguments have been made for Ab against CCR5, a coreceptor for HIV [3, 10, 13]. Furthermore, some clinical studies suggest that CD4-reactive Ab, including a humanized mAb, has therapeutic potential against HIV infection and AIDS progression [5, 8, 10, 12]. However, the development and pathophysiological roles of self-recognizing Ab in healthy individuals are still largely unknown, and a human mAb against CD4 has not yet been isolated.

To gain insights into the genesis of auto-reactive Ab and to characterize the nature of CD4-reactive auto-Ab, we conducted experiments to isolate human monoclonal anti-CD4 Ab from PBMC of 12 HIV-seronegative adult donors. We succeeded in isolating

Correspondence: Dr. Jun Komano
e-mail: ajkomano@nih.go.jp

three independent IgM clones recognizing CD4 from a healthy donor. Analysis of the V-region sequences of CD4-reactive Ab revealed a preference for V gene usage to give rise to CD4-reactive Ab. This is the first report describing CD4-reactive human mAb.

Results and discussion

Isolation of CD4-reactive IgM clones from a healthy individual

PBMC were collected from 12 HIV-seronegative adult volunteers, including two healthy and ten with autoimmune disorders, and B-lymphoblastoid cell lines (B-LCL) were established by infecting the cells with EBV (for experimental procedure, see Supporting Information Fig. 1). B-LCL were propagated in oligoclonal pools. In 790 cultures from one healthy donor, we identified two cultures positive for recombinant human CD4 (rhCD4) reactivity, HO538 and HO702, using ELISA (Fig. 1A). This donor may have a unique Ab repertoire, as auto-reactive B-LCL cultures were identified significantly more frequently in this donor than in the others (Fig. 1A). The rhCD4 reactivity was specific, as no binding was observed to 72 other viral, bacterial, and auto-Ag screened in parallel (Supporting Information Fig. 2). We amplified the Ig genes encoding the Fab regions by RT-PCR and cloned them into the bacterial expression vector pFabI-His2 that produces Fab fragments of an inserted set of V_H and V_L genes. We expected that some clones should reconstitute the CD4-reactive Fab present in the original B-LCL cultures. After screening by ELISA, one CD4-reactive Fab clone, HO538-213, was isolated from the HO538 culture, and two independent clones, HO702-001 and HO702-016, were isolated from the HO702 culture. These Fab clones originated from IgM, as determined by the sequence analysis. The estimated efficiency of peripheral B cells producing CD4-reactive Ab was ~0.0013% (three clones/2.4×10^5 estimated screened B cells × 100 (%), given that the B cells compose 10% of PBMC and that EBV immortalization is 30% efficient on average) [14]. According to the ELISA data, the Fab concentrations that yielded 50% maximal binding were ~8 μg/mL for HO538-213, and ~1 μg/mL for HO702-001 and HO702-016 (Fig. 1B). Consistent with these data, the BIACORE assay revealed that the dissociation constant (Kd) of HO538-213, HO702-001, and HO702-016 to rhCD4 was 6.5×10^{-8}, 7.7×10^{-9}, and 2.7×10^{-9} M, respectively (Fig. 1C), which is relatively weak compared with average Ab–Ag interactions (*e.g.* the Kd of mouse mAb Leu-3a to rhCD4 is 2.2×10^{-10} M).

Genetic analysis of CD4-reactive IgM clones

The Fab sequences were analyzed by the Kabat database (http://www.ncbi.nlm.nih.gov/igblast/) in GenBank, as previously described [15, 16]. The Ig gene family of each gene and the most homologous germline are indicated (Fig. 2A). All the three clones were of the IgM class and had a κ-chain for V_L. Comparison of the

A

Donor	Number of tested cultures	CD4	Nuclear antigen	Blood type i-glycolipid
Healthy 1	790	2 (0.3%)*	21 (2.6%)*	28 (3.5%) *
Healthy 2	160	0	0	0
Autoimmune (10 individuals)	435	0	3 (0.7%)	0

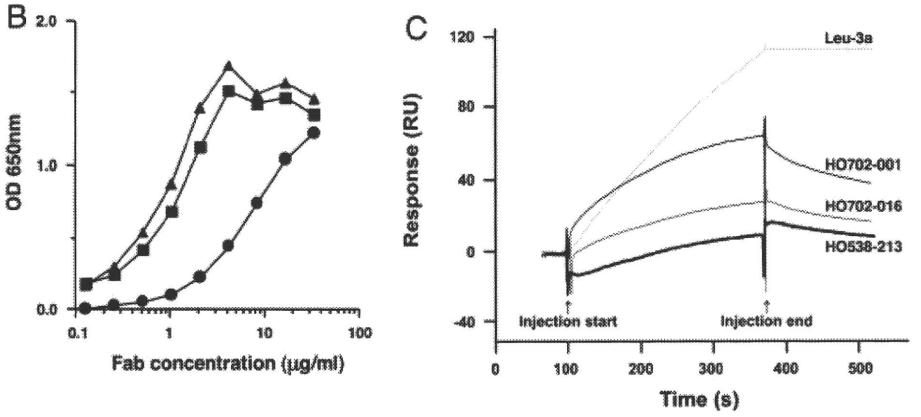

Figure 1. Isolation and characterization of healthy human-derived CD4-reactive Ab. (A) Summary of the frequency of B-LCL cultures that reacted with representative auto-Ag. The number of cultures positive for rhCD4 reactivity, HeLa cell nuclear staining, and blood type i-glycolipid are shown. *$p<0.05$, compared with other donor groups, Fisher's exact test. (B) CD4-binding kinetics of CD4-reactive IgM Fab. Serial dilutions of HO538-213 (circles), HO702-001 (triangles), and HO702-016 (squares) were incubated in microtiter plates pre-coated with rhCD4. (C) Surface plasmon resonance analysis of CD4-reactive IgM FAb HO702-001 (black), HO702-016 (dark gray), HO538-213 (bold), and mAb Leu-3a (gray) binding to immobilized rhCD4. The concentration of Ab was 0.3 μg/mL, flow rate 20 μL/min, and reaction time 270 s. RU, resonance units.

